

1 **Viral transcriptional regulators extensively rewire host pathways through diverse**
2 **mechanisms**

3

4 Jaice T. Rottenberg¹, Xing Liu¹, Anna Berenson^{1,2}, Luis F. Soto-Ugaldi³, Mohamed Y. EISadec⁴,
5 Clarissa Santoso^{1,2}, James E. Corban⁵, Phillip J. Dexheimer^{6,7}, Berkay Engin¹, Ryan Lane¹,
6 Sakshi Shah¹, Kerstin Spirohn-Fitzgerald^{8,9,10}, Shubham Khetan¹¹, Cheng-Che Lee¹, George
7 Munoz-Esquivel¹², Zhaorong Li⁴, Lucia Martinez-Cuesta^{1,13}, Yunwei Lu¹, Philipp Trollmann⁴,
8 Tong Hao^{8,9,10}, S. Stephen Yi^{14,15}, Nidhi Sahni^{15,16}, Martha L. Bulyk^{8,11,17}, Michael
9 Calderwood^{8,9,10}, Matthew T. Weirauch^{6,7}, Marc Vidal^{8,9,10}, Srivatsan Raman^{18,19,20,21}, Juan I.
10 Fuxman Bass^{1,2,3,8,22*}

11

12 ¹ Department of Biology, Boston University, Boston, MA 02215, USA.

13 ² Molecular Biology, Cellular Biology and Biochemistry Program, Boston University, Boston, MA
14 02215, USA.

15 ³ Tri-institutional Program, Computational Biology and Medicine, New York, NY 10065, USA.

16 ⁴ Bioinformatics Program, Boston University, Boston, MA 02215, USA.

17 ⁵ Integrated Program in Biochemistry, University of Wisconsin-Madison, Madison, WI 53706,
18 USA.

19 ⁶ Center for Autoimmune Genomics and Etiology, Cincinnati Children's Hospital Medical Center,
20 Cincinnati, OH, 45229, USA.

21 ⁷ Division of Allergy and Immunology, Cincinnati Children's Hospital Medical Center, Cincinnati,
22 OH, 45229, USA.

23 ⁸ Center for Cancer Systems Biology (CCSB), Dana-Farber Cancer Institute, Boston, MA 02215,
24 USA.

25

26 ⁹ Department of Genetics, Blavatnik Institute, Harvard Medical School, Boston, MA 02115, USA.

27 ¹⁰ Department of Cancer Biology, Dana-Farber Cancer Institute, Boston, MA 02215, USA.

28 ¹¹ Division of Genetics, Department of Medicine, Brigham and Women's Hospital and Harvard
29 Medical School, Boston, MA 02115, USA,

30 ¹² Escuela Profesional de Genética y Biotecnología, Facultad de Ciencias Biológicas,
31 Universidad Nacional Mayor de San Marcos, Lima 15081, Peru.

32 ¹³ Laboratorio de Virología, Centro de Investigación Veterinaria de Tandil (CIVETAN),
33 UNCPBA-CICPBA-CONICET, Campus Universitario, Tandil, Buenos Aires, Argentina.

34 ¹⁴ DLD Comprehensive Cancer Center, Baylor College of Medicine, Houston, TX 77030, USA.

35 ¹⁵ Department of Neurosurgery, Baylor College of Medicine, Temple, TX 76508, USA.

36 ¹⁶ Program in Quantitative and Computational Biosciences (QCB), Baylor College of Medicine,
37 Houston, TX 77030, USA.

38 ¹⁷ Department of Pathology, Brigham and Women's Hospital and Harvard Medical School,
39 Boston, MA 02115, USA.

40 ¹⁸ Department of Biochemistry, University of Wisconsin-Madison, Madison, WI 53706, USA.

41 ¹⁹ Great Lakes Bioenergy Research Center, University of Wisconsin-Madison, Madison, WI
42 53706, USA.

43 ²⁰ Department of Bacteriology, University of Wisconsin-Madison, Madison, WI 53706, USA.

44 ²¹ Department of Chemical and Biological Engineering, University of Wisconsin-Madison,
45 Madison, WI 53706, USA.

46 ²² Biological Design Center, Boston University, Boston, MA 02215, USA.

47

48

49 Correspondence: J.I.F.B. (fuxman@bu.edu)

50

51 **Summary**

52

53 Viral transcriptional regulators (vTRs) reprogram host gene regulatory networks to promote
54 replication, persistence, and immune evasion. Despite the identification of hundreds of vTRs in
55 human viruses, how they rewire host pathways remains unclear. Here, we systematically
56 profiled 95 vTRs from diverse human viruses across multiple functional assays. vTRs perturb
57 immune, cell proliferation/death, and signaling pathways through various mechanisms; some
58 bind DNA directly, others cooperate or antagonize human transcription factors (hTFs), and
59 some remodel chromatin. vTRs can act as activators or repressors and recruit similar but not
60 identical repertoires of proteins as hTFs. These findings reveal vTRs as versatile transcriptional
61 modulators that converge on conserved host “pressure points” while diversifying across
62 pathways to promote viral replication and persistence. Notably, many vTR dysregulate genes
63 within autoimmune, neurological, and cardiovascular risk loci, revealing mechanistic links to
64 disease. Together, we provide a comprehensive resource for understanding and targeting viral
65 control of human transcription.

66

67

68

69 Introduction

70 Viruses are a leading cause of human disease, through direct effects of acute infection and by
71 increasing the risk of chronic conditions, such as multiple sclerosis, dementia, or cancer.¹⁻⁵ A
72 key mechanism underlying viral pathogenicity is the ability to reprogram host gene expression to
73 promote cell states suitable for viral replication or persistence.⁶ In particular, viruses often
74 suppress immune response genes to evade detection and clearance, as well as modulate
75 pathways controlling cell survival and proliferation to prevent elimination of infected cells and
76 enhance viral spread.⁷⁻¹⁰ This viral manipulation of host transcriptional programs likely plays a
77 central role in disease development and progression.

78 Viral proteins can modulate host gene expression either directly—by recruitment to cis-
79 regulatory elements (CREs) in the host genome—or indirectly, by altering signaling pathways
80 that control downstream genes.⁶ Direct modulation typically involves proteins classified as viral
81 transcription regulators (vTRs), which, beyond controlling viral gene expression, can influence
82 host transcription by binding DNA independently, co-binding with human transcription factors
83 (hTFs), or being recruited to DNA via interactions with chromatin-associated proteins such as
84 hTFs or cofactors (**Figure 1A**). For instance, the Epstein-Barr virus (EBV) Zta binds TPA-
85 responsive elements to regulate immune genes,^{11,12} while HBZ from human T-lymphotropic
86 virus 1 (HTLV-1) dimerizes with hTFs JUNB and JUN to modulate their DNA binding activity.¹³
87 In contrast, ChIP-seq studies have shown that vTRs such as EBV EBNA2 are indirectly
88 recruited to human CREs through interactions with hTFs.⁶

89 More than 400 vTRs have been identified in human viruses, predominantly in double-
90 stranded DNA (dsDNA) viruses.⁶ Many vTRs are key mediators of viral pathogenesis, including
91 well-characterized oncoproteins such as E1A from adenovirus, HBx from hepatitis B virus
92 (HBV), and E6 and E7 from human papillomavirus (HPV).¹⁴⁻¹⁶ Other vTRs primarily function as
93 immunosuppressive factors, such as vIRF1-3 and Rta from Kaposi's Sarcoma-associated virus

94 (KSHV).¹⁷ Notably, certain vTRs exhibit allele-specific binding, contributing to the pathogenesis
95 of chronic or complex diseases. For example, the EBV EBNA2 is recruited to nearly half of the
96 genetic risk loci associated with autoimmune disorders such as multiple sclerosis and systemic
97 lupus erythematosus, where it shows evidence of allele-dependent.^{18,19}

98 Despite their critical role in disease, mechanisms of host transcriptional modulation are
99 poorly understood for most vTRs. For instance, genomic occupancy has been mapped for only
100 15 unique vTRs,^{6,20,21} and protein-protein interaction (PPI) data are available for just 74 of the
101 ~400 vTRs.²² Although recent transcriptional activity studies have been systematic, they have
102 focused on 80 amino acid regions,²³ potentially missing larger, synergistic, or context-dependent
103 activation or repression domains. The lack of comprehensive studies comparing various
104 molecular functions of vTRs across diverse viral families has significantly limited our
105 understanding of their regulatory strategies and contributions to pathogenesis.

106 Here, we systematically characterize 95 vTRs from 31 human dsDNA viruses and
107 retroviruses using a multimodal framework to define how vTRs reshape the human
108 transcriptome and uncover the principles governing their regulatory functions. This vTR set
109 spans different structural folds, timing of expression, reported functional roles, and likely
110 mechanisms of action. We find that vTRs from phylogenetically distinct viruses often converge
111 on core host pathways, including immunity, signal transduction, cell division, and apoptosis,
112 revealing both shared and divergent regulatory strategies. This transcriptional rewiring is
113 mediated by distinct mechanisms, including direct DNA binding (independently or cooperatively
114 with hTFs), tethering to hTFs, and active disruption of hTF-DNA binding. We show that vTRs
115 can function as transcriptional activators or repressors and engage in PPI networks that exhibit
116 both shared and unique features compared to hTFs. This integrative analysis reveals previously
117 unappreciated redundancies and division of labor among vTRs encoded by the same virus, as
118 well as striking functional divergence among orthologs. Finally, we identify links between vTR-
119 modulated genes and disease risk loci, suggesting that viral regulators may act as

120 environmental sensitizers of genetic susceptibility. Collectively, our work highlights vTRs as a
121 functionally diverse set of regulators and provides new insights into both viral pathogenesis and
122 fundamental principles of transcriptional control.

123

124 **RESULTS**

125 **vTR1.0: a resource to study the vTR functional landscape**

126 Similar to human transcriptional regulators, vTRs function through direct or indirect recruitment
127 to DNA regions and modulate gene expression through interactions with cofactors and hTFs. To
128 determine the mechanisms by which different vTRs perturb gene regulatory networks, we used
129 an extensive multimodal functional approach integrating transcriptomics, biophysical
130 interactions, and measurements of transcriptional activity (**Figure 1B**). We selected a subset of
131 95 vTRs from the annotated compendium of 419 vTRs for gene synthesis (**Data S1**). These
132 vTRs span all major dsDNA virus and retrovirus families (**Figure 1C**), and include several vTRs
133 known to impact pathogenesis such as E6 and E7 from different HPV strains, EBNA2 from EBV,
134 and E1A from adenovirus. Codon optimized vTR open reading frames were cloned into
135 Gateway compatible donor vectors, resulting in the vTR1.0 entry clone collection, which are
136 easily transferable to destination vectors for different functional assays (**Figures 1B-C**). To
137 determine the effect of vTRs on the human transcriptome, we performed Bulk RNA Barcoding
138 and sequencing (BRB-seq)²⁴ in HEK293T cells transiently expressing 84 different vTRs, of
139 which 58 resulted in altered human gene expression using our stringent criteria (≥ 100
140 differentially expressed genes; $|\text{Log2FC}| \geq 0.5$, $p < 0.05$). To evaluate the intrinsic ability of
141 vTRs to bind to DNA regions (i.e., in the absence of other hTFs), we used enhanced yeast one-
142 hybrid (eY1H) assays, a yeast-based reporter assay that detects protein-DNA interactions
143 (PDIs) in a high-throughput manner. We tested the vTR1.0 collection against a set of 112 DNA-
144 baits derived from the promoter elements (2 kb regions upstream of the transcription start site)
145 of cytokine genes, which are heavily targeted by many viruses.^{25,26} To assess the possible co-

146 binding or sequestration between hTFs and vTRs, we used paired yeast one-hybrid (pY1H)
147 assays, a variation of eY1H that evaluates pairs of proteins for synergistic or antagonistic
148 binding to DNA. In particular, we tested 113 vTR-hTF pairs against 39 immune gene promoters
149 and 83 promoters of genes involved in cell signaling, tumor suppression, oncogenesis,
150 differentiation, metabolism, replication, and apoptosis.

151 To determine the ability of vTRs to activate or repress transcription, we performed
152 mammalian one-hybrid (M1H) assays in HEK293T cells, a method in which proteins are
153 tethered to a firefly luciferase reporter construct to quantify transcriptional activation or
154 repression. Finally, we used yeast two-hybrid (Y2H) assays to screen vTR1.0 against the entire
155 human ORFeome v9.1, comprised of 17,472 protein-coding genes, and identified 132 PPIs
156 between 33 vTRs and 67 human proteins. We maintained a similar viral family representation
157 across assays relative to vTR1.0 (**Figure 1C**) and identified differentially expressed genes,
158 intermolecular interactions, or significant transcriptional activity for 91% of vTRs tested (**Figure**
159 **1D** and **S1**). This illustrates the breadth of functional profiling data generated for our vTR
160 compendium, which is necessary for deriving an integrated picture of vTR function and enabling
161 systematic discovery and comparison of the molecular strategies viruses use to hijack human
162 gene regulation.

163

164 **vTRs modulate multiple host pathways**

165 To determine the pathways rewired by different vTRs, we used HEK293T cells as a
166 standardized human background to allow systematic comparison across the vTRs profiled. This
167 cell line provides high transfection efficiency and stable, well-characterized transcriptional
168 programs, enabling robust detection of vTR-driven perturbations. Moreover, HEK293T cells
169 express a broad set of transcriptional cofactors and signaling components, well-suited for other
170 assays within our multimodal profiling. Importantly, their low basal antiviral response minimizes
171 confounding immune activation, allowing us to quantify vTR-specific effects under basal and

172 stimulated conditions. We expressed individual vTRs in HEK293T cells for 72 hs, determined
173 the transcriptomic profile using BRB-seq, and identified the set of differentially expressed genes
174 relative to empty vector. Gene set enrichment analysis of differentially expressed genes shows
175 that vTRs generally dysregulate pathways associated with immune response, apoptosis, cell
176 cycle, DNA damage repair, and metabolism (**Figure 2A**). These pathways have been broadly
177 associated with viral replication and persistence, and some are known to be affected by vTRs;
178 for example KSHV vIRFs are known to inhibit p53 activity.^{27,28} Consistent with this, vIRF1/3/4
179 downregulated several pathways associated with p53 regulation, as well as downstream
180 pathways including those regulating cell cycle checkpoints and DNA double-stranded break
181 repair (**Figure 2A**). Similarly, HPV E6 and E7, commonly associated with suppression of
182 apoptosis and innate immunity and the upregulation of cell cycle genes,^{29,30} substantially
183 modulated these pathways.

184 We next evaluated whether vTRs from the same viral family, vTR homologs from related
185 viruses, and vTRs from the same virus broadly affect similar or different pathways. To
186 accomplish this, we calculated the Pearson correlation coefficient of pathway normalized
187 enrichment scores for each pair of vTRs, which were rescaled using the connection specificity
188 index (CSI) that ranges from 0 (anti or not correlated) to 1 (highly correlated).^{31,32} We observed
189 that vTR pairs have an overall low correlation between affected pathways, consistent with the
190 diverse functions and pathways affected by different vTRs, whereas homologous vTRs and
191 vTRs from the same virus have more similar transcriptional effects (**Figure 2B**). The broad
192 distribution of correlation values between vTRs from the same virus, however, suggests that
193 division of labor, redundancy, cooperation, and opposing effects between vTRs may all be
194 employed by viruses to robustly rewire host cellular pathways. For instance, E1A and IVa2 from
195 adenovirus A exhibit opposite regulation of signal transduction and RNA processing related
196 pathways and mutually exclusive regulation of cell cycle (E1A) and metabolism (IVa2) (**Figure**
197 **2C** and **Data S2**). The contrasting transcriptional effects of these two vTRs combined with their

198 distinct expression kinetics (E1A - immediate early, IVa2 - late) underscore the unique
199 requirements for each progressive stage of adenovirus infection. Conversely, IE1 and IE2, both
200 expressed from the human cytomegalovirus (HCMV) major immediate early promoter, have
201 highly concordant effects on host pathways (**Figure 2D**), including upregulation of signal
202 transduction and downregulation of metabolism pathways. Together, this illustrates how vTRs
203 from the same virus may have similar or different transcriptional effects depending on their
204 expression timing during infection.

205 Interestingly, we identified 70 vTR-pairs that produce highly similar transcriptional
206 profiles (CSI > 0.9) from viruses belonging to different viral families. For example, HPV-5 E2
207 and HCMV UL34 (**Figure 2A**), upregulate pathways involved in cell-cell communication and
208 downregulate those associated with cell cycle control and DNA damage repair (**Figure 2E**). This
209 marked degree of pathway similarity between HPV-5 E2 and HCMV UL34, as well as other
210 vTRs with similar transcriptional profiles, is not attributable to similarities in structure (**Figure**
211 **2F**). Together, these results illustrate how vTRs from distant, unrelated viruses can have similar
212 transcriptional effects, suggesting that viruses have converged to affect overlapping host
213 pathways while retaining specific effects on viral gene regulation.

214 More generally, we found 5 clusters of vTRs with overall similar transcriptional profiles
215 (**Figure 2A**). As expected, homologous vTRs are generally clustered together, illustrating the
216 quality of our clustering approach. Of the clusters identified, Clusters 2 and 3 are notable for
217 exhibiting somewhat opposite effects. vTRs from Cluster 2 downregulate genes involved in
218 cellular stress such as apoptosis, DNA damage response, hypoxia, and chemical stress, and
219 those related to cell replication, and upregulate immune, cell-cell communication, and
220 intracellular signaling pathways. Instead, vTRs in Cluster 3 include many oncoproteins (e.g,
221 HPV-18 E6, HPV-16/HPV-5 E7, and HTLV-1 Tax^{4,33} and upregulate pathways related to cell
222 cycle progression, DNA damage, and stress responses, while downregulating those involved in
223 extracellular signaling and antigen presentation. Interestingly several viruses, such as HPV and

224 EBV, encode vTRs present in both Clusters 2 and 3, suggesting potential balancing
225 mechanisms controlling cell growth and stress at different stages in the viral replication cycle. In
226 addition, each cluster is composed of vTRs from different viruses and families. Together, our
227 results suggest that unrelated viruses have evolved convergent transcriptional strategies to
228 manipulate common host processes, while retaining distinct programs tailored to their specific
229 requirements for persistence and replication.

230

231 **vTR regulation of pathways in infected cells**

232 Viral infection greatly affects cell states and signaling pathways, some of which are leveraged
233 by the virus to promote replication or persistence, while others reflect host antiviral responses.
234 To determine how vTRs function in infected cells, we performed BRB-seq in HEK293T cells
235 infected with Sendai virus (SeV) following transient transfection of 49 vTRs. We found that vTRs
236 often regulate similar pathways regardless of infection state (**Figure 2G**), suggesting that the
237 function of most vTRs is robust to antiviral mechanisms. However, 12 vTRs affect different
238 pathways in infected versus uninfected conditions, and in some cases have opposite effects.
239 For instance, VLTF-3 (vaccinia virus) shifts from repressing to activating metabolic/biosynthetic
240 pathways and from activating to repressing cell cycle pathways in SeV-infected cells (**Figure**
241 **2H**), which may enable the virus to adapt to different cellular states.

242 Several vTRs, including IE1 (HCMV) and KSHV vIRFs, are known to act as
243 immunomodulatory proteins.³⁴⁻³⁶ To identify additional vTRs that may counteract the antiviral
244 effects elicited by infection, we focused on 45 pathways that are altered under SeV infection
245 relative to resting cells, including interferon response, interleukin signaling, NF- κ B activation,
246 and antigen presentation. We identified 47 vTRs that affect at least one of these pathways in
247 SeV-infected cells (**Figure 2I**), of which 39 downregulate immune-associated pathways normally
248 upregulated in the presence of SeV. While several of these associations are known, such as
249 vIRF-1 affecting interferon pathways^{36,37} and IE1/2 downregulating the T-cell receptor and

250 interleukins,^{34,35} our results also identify several novel immunoregulatory functions. For
251 example, Tax proteins from HTLV-2 and HTLV-3, typically associated with NF- κ B regulation,³⁸
252 both downregulate type I interferon signaling, whereas DR7L (HHV-6A) and IE63 (Varicella-
253 Zoster virus - VZV) downregulate IL-1-associated pathways (**Figure 2I**). In addition to
254 immunomodulatory roles, 31 vTRs upregulate signaling pathways normally suppressed during
255 active infection (**Figure 2I**), which may reflect indirect immune evasion strategies that attempt to
256 reestablish cellular processes needed for replication. Together, these findings reveal that vTRs
257 not only buffer against infection-induced stresses but also actively reshape antiviral signaling.

258

259 **vTRs are recruited to host DNA through multiple mechanisms**

260 Transcriptional regulators can be recruited to DNA elements using different mechanisms,
261 including direct binding to DNA (either independently or as part of a protein complex) and
262 indirect recruitment mediated by DNA-binding factors. We previously curated 33 ChIP-seq data
263 sets corresponding to 12 vTRs, which showed large variations in target preference and binding
264 distance to transcription start sites.⁶ This study showed that ChIP-seq peaks of many vTRs are
265 enriched for hTF motifs, suggesting indirect recruitment of vTRs to genomic sites. Other vTRs
266 have been shown to bind DNA directly, including bZIP Zta (EBV) and E2A (adenovirus).^{12,39}

267 To identify which vTRs are recruited to DNA directly and through which mechanisms, we
268 first used PADIT-seq⁴⁰ to assay the DNA binding activities of ten vTRs to all possible 10-bp
269 DNA sequences. These vTRs were selected based on their likelihood of directly binding to DNA
270 given domain presence (e.g, viral IRFs), Y1H data, or previous vTR-DNA interaction data.²⁶ To
271 facilitate protein expression, we expressed structured vTR regions and 10-15 flanking amino
272 acids, as previously conducted for hTFs.⁴⁰ However, none of these vTR constructs showed
273 significant binding to 10-bp DNA sequences, while our hTF positive controls did. The observed
274 lack of DNA binding activity may be due to misfolding of the vTRs in the *in vitro* transcription and
275 translation system, the need for excluded vTR regions, or interference by the ALFA tag fusion

276 required by the assay, that these vTRs can only bind sequences longer than the 10-mers tested
277 in PADIT-seq, or that the vTRs associate indirectly, rather than directly, with their target
278 genomic sites.

279

280 To address these possibilities, we performed eY1H assays which evaluate interactions
281 between individual proteins and DNA regions of up to 2 kb in the absence of other human or
282 viral proteins. We tested 95 vTRs against 112 immune gene promoters, given that most vTRs
283 dysregulate at least one immune pathway. We also assessed cooperativity with hTFs using
284 pY1H assays, a modified eY1H approach that evaluates DNA binding of protein pairs. We
285 tested 113 vTR-hTF pairs selected based on reported PPIs, homologs of known vTR-hTF
286 interactions, and PPIs identified in this study. Both individual vTRs/hTFs and their pairs were
287 assayed against 39 cytokine promoters and 83 promoters of genes from the Cancer Gene
288 Census, involved in cell proliferation, cell death, and cell signaling, all pathways dysregulated by
289 vTRs (**Figure 2A**).

290 We identified 17 vTRs (18% of vTRs tested) that bind human promoters (**Figure 3A** and
291 **Data S3** and **S4**). This is similar to the proportion of hTFs binding these regions (24%),²⁵
292 suggesting that many vTRs might not rely on hTFs for DNA recruitment, in contrast to previous
293 studies.⁶ Vaccinia VLTF-1 and hepatitis B X-protein (HBx) have the most DNA targets, with 39
294 and 14 PDIs respectively. In addition to the established HBx target *TNF*,⁴¹ HBx binds the *MYC*
295 promoter, suggesting direct regulation, consistent with reports of HBx-associated increases in
296 *MYC* expression and activity in hepatocellular carcinoma, though direct control had not been
297 shown.^{42,43} We also found HBx binding to the promoter of *LEF1*, a key hTF controlling Wnt
298 signaling, in line with our transcriptomics data showing HBx upregulates several Wnt signaling
299 pathways and with previous studies that implicate HBx in regulating host Wnt signaling during
300 the progression of hepatocellular carcinoma.^{44,45}

301 We also identified 9 vTRs that bind DNA cooperatively with hTFs (**Figure 3A-B**). For
302 example, we observed co-binding between bZIP HBZ (HTLV-1) and the human bZIP DDIT3 at
303 the *MYC* and *FGFR3* promoters (**Figures 3C**), two genes heavily involved in oncogenic
304 pathways. This is consistent with studies showing that HTLV-1 activates *MYC* expression in
305 adult T-cell leukemias.⁴⁶ We also found cooperative interactions between HPV-5 E6 and IRF3 at
306 the *IFNB1* promoter, and between HPV-5 E7 and IRF1 at the *IFNL1*, *IL15*, and *TNFSF10*
307 promoters (**Figure 3D**), in line with known immunomodulatory roles of E6 and E7.⁴⁷⁻⁴⁹
308 Considering that E6 and E7 are known to inhibit transcriptional activation by IRF3 and IRF1,
309 respectively,^{49,50} our results suggest that E6 and E7 may outcompete IRF dimers to prevent
310 activation of immune response genes. Interestingly, HPV-16 E7 cooperatively binds to DNA with
311 ZNF398 (**Figure 3E**), an oncogenic hTF that promotes tumorigenesis through p53 degradation,
312 enhanced cellular metabolism, disruption of ferroptosis, and maintenance of cancer stem cell
313 niches.⁵¹⁻⁵⁵ Our results suggest that E7 may leverage these ZNF398 functions to promote cell
314 proliferation and prevent cell death.

315 In addition to the detected vTR binding events, we observed 12 vTR-hTF pairs in which
316 a vTR antagonized the binding of a hTF at specific promoters (**Figure 3B**). This likely occurs by
317 sequestration, as AlphaFold3 modeling predicts binding of the vTRs to the DNA binding domain
318 of the interacting hTFs (**Figure S2**). For example, E2F4 is antagonized by several HPV E7
319 orthologs, which are predicted to interact with the DNA-contacting interphase of the E2F domain
320 (**Figure 3B, F, G**). Ingenuity pathway analysis of our BRB-seq data shows that expression of
321 HPV-16 E7 leads to downregulation of E2F targets (z-score = -2.164, p = 0.0022). HPV E7 is
322 known to bind the tumor suppressor retinoblastoma gene (RB1) and prevent its association with
323 E2F proteins.^{56,57} Together with our results, this suggests that E7 may disrupt E2F function
324 through two separate mechanisms: inhibition of RB1-E2F association and sequestration of E2F,
325 preventing its association with DNA. We observe a similar pattern for TFAP2A, which was

326 antagonized by HPV-16 E7 at 15 promoters (**Figure 3B**) and was previously shown to be
327 downregulated in cervical cancer cell lines expressing E7.⁵⁸

328 We also observed 36 instances in which HCMV IE2 antagonized the DNA binding of
329 ZNF281 likely by forming an interlocked complex between both proteins that occludes the
330 cys2His2 zinc fingers of the DNA binding domain (**Figures 3B, 3H, S2, and S3**). ZNF281 is an
331 oncogenic hTF associated with several types of cancer and plays a role in inflammation.^{59–62} By
332 preventing ZNF281 binding to its normal targets, IE2 may redirect ZNF281 either to the HCMV
333 genome or to other host gene promoters. Interestingly, we detected a cooperative interaction
334 between IE2 and ZNF281 at the *IL1B* promoter (**Figures 3B and 3G**). Although IE2 is primarily
335 an activator, we propose that recruitment of ZNF281 may result in a repressive complex.
336 Indeed, we observed that IE2 repressed IL1-related pathways in our transcriptomics data from
337 SeV-infected cells (**Figure 3I**). Our results suggest a novel regulatory mechanism by which IE2
338 co-opts ZNF281 to suppress interleukin response during active infection states. This
339 mechanism is distinct and complementary to reported immune suppressor activities of IE2
340 mediating STING and CD83 degradation, activation of the IL10/STAT3 signaling pathway, and
341 inhibition of antigen presentation.^{63–66}

342 Together, our results extend previous reports on vTR recruitment to host DNA and show
343 that in addition to indirect and independent DNA binding, vTRs may reprogram host gene
344 expression through cooperative or antagonistic interactions with hTFs (**Figure 3J**). Interestingly,
345 we show that 18 vTRs may modulate expression through multiple mechanisms, potentially
346 expanding their regulatory targets (**Figure 3J**). This is likely an underestimate given the limited
347 number of DNA sequences tested by Y1H assays and the sparsity in currently available vTR
348 ChIP-seq datasets. Altogether, our data uncover an unexpectedly broad repertoire of DNA-
349 engagement mechanisms, showing that vTRs can operate as independent DNA binders,
350 partners that co-opt hTFs, or antagonists that block hTF interactions, often combining multiple
351 modes to rewire host gene expression.

352

353 **vTRs alter chromatin accessibility**

354 In addition to binding to open regions in the host genome, vTRs can drive changes in chromatin
355 architecture. While these effects have been demonstrated for several vTRs including
356 Adenovirus E1A, EBV BZLF1, and HIV Tat,^{67–69} the effects of many vTRs on chromatin
357 accessibility remain largely uncharacterized. We performed PROD-ATAC, a single-cell ATAC-
358 seq approach that evaluates the effect of protein overexpression on chromatin accessibility
359 (39048711), to determine the accessibility landscapes generated by EBV EBNA3A and
360 EBNA3B, Adenovirus B E4ORF6/7, and HBV X-protein expression in HEK293T cells (**Figure**
361 **S4A**). Of these vTRs, EBNA3A produced the largest number of differentially accessible peaks
362 (**Figure 3K**), with newly opened regions enriched for PBX, CDX, and HOX motifs (**Figure 3L**).
363 This is consistent with a recent study showing that EBNA3A ChIP-seq peaks and newly opened
364 regions (ATAC-seq) are enriched for PBX motifs.²⁰ We also found that regions closed in
365 EBNA3A expressing cells are enriched for HOX and CDX motifs, though these regions are
366 different from those with HOX/CDX motifs opened in EBNA3A-expressing cells, suggesting that
367 EBNA3A induces the remodeling of chromatin occupied by different homeodomain proteins.

368 We also detected marked changes in accessibility by Adenovirus B E4ORF6/7, which
369 exhibit minimal overlap with those driven by EBNA3A (**Figure 3K**). Newly opened chromatin
370 induced by E4ORF6/7 was enriched for p53/p63 motifs (**Figure 3M**), whereas closed regions
371 were dominated by HOX/CDX motifs. E4ORF6/7 has been reported to interact with p53;
372 however, unlike its larger splice variant E4ORF6, it does not degrade p53.^{70,71} Together with our
373 results, this supports a model in which E4ORF6/7 promotes occupancy of p53 binding sites,
374 potentially modulating p53 targets. Indeed, ingenuity pathway analysis shows that Adenovirus B
375 E4ORF6/7 expression leads to the upregulation of p53-responsive genes (z-score = 2.092, p =
376 4.2x10⁻⁵). Interestingly, both E4 splice variants are co-expressed early during infection,
377 although E4ORF6/7 is less stable,⁷² suggesting that the adenoviral lifecycle may require distinct

378 regulation of p53 (e.g. degradation/transcriptional regulation) at specific time points during
379 infection.

380

381 **vTRs have intrinsic transcriptional effector activity**

382 Like hTFs, many vTRs contain effector domains that recruit transcriptional cofactors to activate
383 or repress target gene expression.⁷³ A previous study using HT-recruit, a high-throughput tiling
384 peptide approach to screen for transcriptional activity, identified hundreds of viral effector
385 domains.²³ Because effector domains may function differently in the context of a full-length
386 protein structure, and because some effector domains can be larger than those examined using
387 HT-recruit (80 amino acids),^{74,75} we interrogated the transcriptional activity of 95 full-length vTRs
388 using M1H assays. M1H uses a luciferase reporter downstream of an enhancer element that
389 contains 4 copies of the Gal4 upstream activating sequence (UAS). A protein (e.g., a full-length
390 vTR) fused to the Gal4 DNA binding domain is then recruited to the reporter construct and may
391 activate or repress luciferase expression. We used two versions of the M1H assay, using either
392 a minimal or a moderate promoter between the UAS and luciferase, to better capture both
393 activation and repression. Using our minimal promoter system, we observed that 25.2% of vTRs
394 tested are strong transcriptional activators ($\text{Log}_2(\text{fold change}) \geq 5$), compared to only 6.75% for
395 a set 224 hTFs with broad representation across families and that was evaluated using the
396 same M1H system (**Figure 4A**).⁷⁶ This suggests that vTRs may have evolved potent effector
397 functions, enabling viruses to more effectively reprogram viral and host transcriptional networks.

398 Using our moderate promoter M1H system, we identified 36 activator and 13 repressor
399 vTRs (**Figure 4B** and **Data S5**). We observed different distributions in vTR activity across viral
400 families. Many highly active vTRs belong to herpesviruses or adenoviruses, the latter of which
401 also account for half of repressive vTRs. Comparatively, poxvirus, papillomavirus, and retrovirus

402 vTRs show milder transcriptional effects, which may reflect different roles in direct regulation of
403 transcription.

404 We next compared the transcriptional activity of vTRs expressed at different stages of
405 the viral lifecycle, and observed striking differences in activity between these groups (**Figure**
406 **4C**). Immediate-early vTRs, which play integral roles initiating viral expression cascades, have
407 the highest activity among all groups. We also observed that many vTRs expressed late in the
408 lytic cycle act as repressors rather than activators. Notable exceptions are highly active
409 tegument proteins UL48 (HHV-1/2) which, although lately expressed, initiate transcription of
410 immediate-early genes upon infection or reactivation (**Figure 4C**).⁷⁷ Finally, vTRs expressed
411 during latency exhibit low levels of transcriptional activity, suggesting that these vTRs may elicit
412 more subtle or context-specific effects on viral and host expression to favor persistence.

413

414 **vTRs interact with overlapping but distinct sets of proteins compared to hTFs**

415 hTFs regulate gene expression through interactions with cofactors, chromatin modifying
416 enzymes, other hTFs, and members of the transcription preinitiation complex.⁷⁸⁻⁸² To identify
417 potential mechanistic similarities and differences between vTRs and hTFs, we compared their
418 PPI profiles. Many PPIs between viral and host proteins were previously determined,^{22,83,84}
419 mostly using affinity-based methods such as IP-MS; however, these methods are biased
420 towards abundant proteins and often identify indirect interactors. Because we expected vTRs to
421 interact with hTFs, which are generally lowly abundant, we performed Y2H assays, which do not
422 depend on *in vivo* protein abundance as proteins are expressed using a defined promoter. We
423 performed Y2H assays between each vTR in the vTR1.0 collection and the complete human
424 ORFeome (~17,500 proteins). Positive hits were retested pairwise in a matrix format to enable
425 PPI comparisons between vTRs. In total, we identified 132 PPIs between 33 vTRs and 67
426 human proteins, 13 of which had been identified in earlier studies (**Figure 1D** and **Data S6**).

427 After integrating our Y2H with available PPI data, we observed that 31.2% of vTR
428 interactions involve hTFs or cofactors, significantly more than for other viral proteins and similar
429 to hTFs (**Figure 4D-E**). Strikingly, we detected previously unreported interactions between six
430 vTRs and the cofactor TLE5 via Y2H assays (**Figure 4F**). TLE5 belongs to the TLE family of
431 transcriptional co-repressors, which regulate proliferation, survival, cell fate, and immunity.^{85,86}
432 Unlike other TLE proteins, TLE5 lacks repression domains and instead acts as a dominant-
433 negative regulator interfering with repressive complex formation.⁸⁵⁻⁸⁷ We found that US1 (HHV-
434 1), UL83 (HCMV), E7 (HPV-16), and Tax (HTLV-1), with available BRB-seq data, altered
435 pathways typically regulated by TLE proteins, including Notch and Wnt signaling, and RUNX
436 target genes (**Data S2**). We confirmed TLE5 interactions with US1 (HSV-2) and UL82 (HCMV)
437 by co-immunoprecipitation and western blot (**Figure 4G**). Structural modeling of these
438 interactions with Alphafold3 showed that both US1 and UL82 associate with the Q-domain of
439 TLE5 (**Figure 4H**), which is required for interaction with other TLE proteins.^{86,87} This suggests
440 that many vTRs from different viral families sequester TLE5 away from other TLE family
441 members, thereby disrupting host transcriptional repression. Beyond TLE5, many other vTRs
442 also modulate Notch and Wnt signaling pathways likely through alternative mechanisms,
443 implicating these pathways as critical for viral replication or immune evasion (**Figure 2A** and
444 **Data S2**).

445 Strikingly, over 60% of vTRs with at least 3 PPIs predominantly interact with non-
446 TF/cofactor proteins (**Figure 4I**). This suggests a spectrum of vTR functionality beyond direct
447 transcriptional regulation, consistent with the known multifunctionality of viral proteins including
448 vTRs.⁶ For instance, early vTRs interact with proteins involved in proteostasis, signaling, and
449 metabolism, aligned with their role in manipulating the host cell environment for viral replication
450 (**Figure 4J**). Latent vTRs interact with immune, RNA processing, metabolic, and proteostatic
451 proteins, potentially contributing to regulate cellular states, evade antiviral responses, and
452 preserve latency.

453 Next, we evaluated which individual human proteins preferentially interact with vTRs or
454 hTFs. As expected, many hTFs, cofactors, and RNA processing proteins preferentially interact
455 with hTFs (**Figure 4K**). Similarly, a set of 14 proteins, consisting primarily of broadly expressed
456 cofactors (e.g., EP300, CREBBP, and KAT2B) and hTFs (TP53, SP1, and CEBPB), was found
457 to frequently interact with both hTFs and vTRs. We also found 40 proteins biased towards
458 interactions with vTRs. This includes basal hTFs such as TBP and GTF2B, MEOX1 known to
459 influence development, and NR4A1, RB1 and CCNA2, involved cell cycle control and cell
460 death.⁸⁸⁻⁹⁴ We also found that proteins involved in proteostasis, cell signaling, metabolism, and
461 immunity preferentially interact with vTRs rather than hTFs (**Figure 4K**), consistent with the
462 multifunctionality of vTRs.⁶

463 Proteins with similar PPIs often share molecular functions. We therefore examined
464 whether any vTR would engage in similar PPIs to those of a hTF, which could indicate
465 convergent regulatory strategies. As expected, we observed enrichment of vTR homologs and
466 hTF paralogs among vTR-vTR and hTF-hTF pairs with similar PPIs (**Figure 4L**); however, hTFs
467 and vTRs engage broadly distinct sets of host proteins and we detected no hTF-vTR pair with
468 similar PPIs (Jaccard>0.3, **Figure 4M**). This underscores that vTRs have evolved unique
469 interaction networks rather than mirroring those of hTFs.

470

471 **Redundancy and division of labor between vTRs from the same virus**

472 Large dsDNA viruses such as herpesviruses encode multiple vTRs that regulate diverse viral
473 and host processes.⁶ To better understand the division of labor between vTRs from the same
474 virus, we compared the overall host transcriptional effects of vTRs from viruses with two or more
475 vTRs in our BRB-seq dataset. vTRs from the same virus range from affecting highly similar to
476 highly dissimilar pathways under both resting and SeV-infected conditions (**Figures 5A-B**).
477 Similarity in pathways affected is not necessarily related to timing of vTR expression (**Figure**
478 **5C**). For example, LMP1 and EBNA3A from EBV, both expressed primarily during latency,

479 affect similar pathways to the lytic gene BZLF1, mostly driven by cell cycle, DNA damage, and
480 immune/stress pathways (**Figure 5D-E**). By contrast, EBNA3A, EBNA3B, and EBNA3C, which
481 are generated by alternative splicing from a single latently expressed transcript,⁹⁵ exert distinct
482 effects on host gene expression (**Figures 5D-E**). In contrast to EBV, HCMV vTRs expressed at
483 the same time during infection exhibit the most correlated transcriptional effects (**Figure 5F**).
484 For instance, immediate early IE1 and IE2 affect similar cell cycle, DNA damage, metabolism,
485 and immune/stress pathways, whereas early UL34 and UL82 regulate cell cycle and
486 immune/stress genes (**Figures 2D** and **5G**). Together, this suggests that vTRs from the same
487 virus often co-regulate pathways, which is not necessarily related to the timing of vTR
488 expression. These observations are consistent with a recent study showing that latent EBNA2
489 and lytic switch Rta from EBV share many gene targets during distinct stages of infection.²⁰

490 vTRs from the same virus can also engage in division of labor, with individual vTRs
491 preferentially influencing specific host pathways or exerting distinct effects across cellular
492 conditions. For instance, while LMP1, Zta, and EBNA3A affect similar cell cycle, DNA damage,
493 and immune/stress pathways, they differ in the particular metabolic pathways affected (**Figure**
494 **5E**). Other vTRs, instead, modulate shared or distinct pathways depending on particular cellular
495 conditions. For example, UL48 and UL54 (HHV-2), which are highly concordant in non-infected
496 cells (CSI = 0.9) diverge under SeV infection (CSI = 0.13), whereas 99R and VITF-3 (Tanapox)
497 affect different pathways in non-infected conditions, but similar pathways under SeV infection
498 (CSI = 0 uninfected cells; CSI = 0.73 infected cells) (**Figure 5B**). Together, this illustrates both
499 partial redundancy and specialization between vTRs from the same virus in rewiring host gene
500 regulation networks, which overall results in an expanded set of pathways affected (**Figure 5H**).

501

502 **vTRs from the same virus interact with similar host proteins**

503 We next evaluated whether the overall shared pathways between vTRs from the same virus
504 (**Figure 2B**) can be attributed to similar interactions with host proteins. We observed that vTRs

505 from the same virus tend to have higher interaction profile similarity than vTRs from different
506 viruses, suggesting partial overlap in their regulatory targets or reliance on similar host
507 pathways during infection (**Figure 5I**). To explore how multiple vTRs from a single virus may act
508 in concert, we examined host proteins interacting with at least three vTRs from the same virus in
509 our dataset (**Figure 5J**). In line with the overall enrichment of transcriptional cofactors among
510 vTR targets, KSHV and EBV vTRs interact with CREBBP and EP300, whereas HPV-5 vTRs
511 bind to TBP. Beyond transcriptional regulators, we identified shared interactions involving
512 diverse cellular processes: HHV-1 vTRs associate with the immune sensor IFI16, HPV-18 vTRs
513 engage the cytoskeletal and autophagy-related protein MAP1S, and EBV vTRs collectively
514 interact with host factors linked to signaling, apoptosis, immune responses, and metabolism
515 (**Figure 5J**). These observations indicate that vTRs from the same virus can converge on
516 common host interaction hubs, suggesting coordinated modulation of cellular pathways during
517 infection.

518

519 **vTR homologs display varying levels of functional divergence**

520 Homologous viral genes range from functionally conserved to highly divergent, reflecting
521 selective pressures for either conservation or adaptation to specific tropisms and hosts. We
522 compared 19 sets of vTR homologs across our experimental modalities (**Figure 6A**). Despite an
523 overall high correlation in transcriptional effects between homologous vTRs relative to random
524 vTR-pairs in our BRB-seq dataset (**Figure 2B**), homologs display varying levels of similarity
525 (**Figure 6B**). For instance, HTLV Tax proteins are highly correlated with each other, sharing
526 many regulated pathways in both uninfected and infected conditions. By contrast ICP22
527 homologs from alpha-herpesviruses (HHV-1 US1, HHV-2 US1, and VZV IE63) affect different
528 pathways, with VZV IE63 being the most different, consistent with the evolutionary distance
529 between VZV and HHV-1/2. In particular, HHV-1 and HHV-2 US1 both downregulate similar
530 metabolic pathways, while these are upregulated by VZV IE63. All three ICP22 homologs,

531 however, have very different effects on cell-cell signaling pathways (**Figure 6C**). While HHV-1
532 US1 mostly downregulates pathways associated with extracellular signaling, HHV-2 US1 and
533 VZV IE63 frequently upregulate them; however, the identity of these upregulated pathways
534 generally differs (**Figure 6C**).⁹⁶ The pathways exclusive to HHV-2 US1 are largely involved in
535 cell growth and metabolite trafficking, whereas VZV IE63 upregulates pathways associated with
536 extracellular matrix organization and interaction between cells. Unlike HHV-1/2, where
537 transmission is mediated by virion release and entry, VZV is mostly transmitted through cell-to-
538 cell contact.^{97,98} Thus, targeted regulation of host pathways facilitating cell-cell contact by VZV
539 IE63 and not other alpha-herpesvirus ICP22 homologs underscores a major difference in
540 pathology and transmission of these three viral species.

541 As expected, CSI transcriptional similarity is generally correlated with amino acid
542 sequence identity between homologs (**Figure 6D**). However, there are several exceptions
543 involving dissimilar vTR homologs affecting similar pathways. For instance, while E7 from HPV-
544 5 and HPV-16 only share 35% amino acid identity, their CSI similarity is 0.85. Similarly, E7 from
545 HPV-1 and HPV-2 have a CSI similarity of 0.66 with a sequence identity of 41%; however, these
546 E7 proteins affect different pathways than those affected by E7 from HPV-5 and HPV-16,
547 including cell-cell signaling, cell cycle, DNA damage response, and RNA processing (**Figure**
548 **6E**). We also found that the highly dissimilar E2 from HPV-16 (high-risk of cancer) and HPV-5
549 (low-risk) elicit a very similar transcriptional response in unstimulated cells (31% sequence
550 identity; CSI = 0.99). However, while HPV-16 E2 maintains a robust transcriptional effect upon
551 SeV infection, upregulating extracellular signaling and downregulating cell cycle pathways,
552 infection flips the HPV-5 E2 transcriptional effect (**Figure 6F-G**). These differences in responses
553 to SeV infection were also observed for other sets of vTR homologs (**Figure 6H**). Altogether,
554 this suggests that different viral species may share functions between some but not other vTR
555 homologs, potentially contributing to differences in infection severity and outcomes.

556 hTF effector domains evolve rapidly, often resulting in differences in activity levels or
557 sign between homologs.⁷³ To determine whether these differences are observed for vTRs, we
558 compared the M1H transcriptional activity within homolog groups (**Figure 6I**). We identified
559 several groups containing both activating and repressing vTRs such as HPV E6 and adenovirus
560 E2A (**Figure 6I**). These homologs showed marked PPI differences (**Figures 6J-K**). The
561 activating adenovirus B E2A interacts with proteins commonly associated with transcriptional
562 activation, including MAPK8 and MAPK9, whereas the repressive adenovirus F E2A interacts
563 with chromatin modulator PAXIP1 and transcription factor ZNF446, which contains a strong
564 repressive KRAB domain (**Figure 6J**). Similarly, repressive HPV-1 E6 associates with co-
565 repressors TRIM28 and SUZ12 (**Figure 6K**). Interestingly, E6 from both HPV-16 and HPV-18
566 do not exhibit strong transcriptional activity by M1H assays, despite interacting with strong
567 coactivators such as CREBBP and EP300 (**Figure 6K**). In comparison, HPV-5 E6 is highly
568 active and associates with CREBBP, EP300, as well as the coactivators MAML1 and TADA3
569 (**Figure 6K**). MAML1, typically linked to NOTCH signaling, binds CREBBP and enhances
570 histone acetyl-transferase activity,⁹⁹ while TADA3, a component of the PCAF complex, bridges
571 EP300 and CREBBP.¹⁰⁰ This suggests that MAML1 and TADA3 may help stabilize
572 EP300/CREBBP function and support the transcriptional activation conferred by HPV-5 E6.
573 Together, these data suggests that vTR homologs can have opposite transcriptional effects
574 driven by differences in interactions with coactivators, corepressors, and hTFs.

575 Certain homolog groups, including adenovirus E1A and E4ORF6/7, HPV E7, and
576 herpesvirus VP16 activate transcription, though at varying magnitudes. Yet, homologs within
577 each of these groups affect the expression of different pathways (**Figure 6B and 2A**), likely by
578 regulating different target genes. Indeed, homologs of HPV E6 and E7 show different DNA
579 binding profiles by Y1H assays (**Figure 3A**). In addition, we found marked differences in
580 chromatin accessibility between homologs of adenovirus E4ORF6/7 by PROD-ATAC, with
581 adenovirus B E4ORF6/7 exhibiting the broadest and strongest increase in accessibility (**Figure**

582 **6L** and **S4A**). This is also consistent with adenovirus B E4ORF6/7 affecting the expression of
583 ~5-fold as many genes as other E4ORF6/7 orthologs (**Figure S4B**). Despite differences in
584 genomic position and degree of accessibility, regions of open chromatin detected upon
585 expression of E4ORF6/7 homologs are similarly enriched for p53/p63 motifs, suggesting that
586 binding differences may be linked to differences in PPI strengths, cooperative DNA binding, or
587 pioneering effects (**Figure 6M**). Collectively, these results show that although vTR homologs
588 often share certain functions, they frequently diverge in others, leading to distinct patterns of
589 host target engagement, transcriptional outcomes, and possibly other molecular activities.

590

591

592

593 **vTRs regulate genes associated with disease risk**

594 Viral infections have long been associated with different chronic diseases, including
595 autoimmune and neurological disorders, through molecular mimicry, bystander activation,
596 immune dysregulation, and alteration of immune tolerance.^{101,102} For instance, numerous studies
597 have shown that EBV EBNA2 is recruited to the risk loci of multiple autoimmune diseases
598 through interactions with hTFs such as RBPJ, leading to host gene dysregulation.^{18,103,104,105} To
599 determine whether this is a unique feature of EBNA2 or whether other vTRs may also alter the
600 expression of genes at disease risk loci, we evaluated the overlap between genes modulated by
601 each vTR and risk loci from genome-wide association studies (GWAS). In total, we identified 40
602 vTRs with significant associations (FDR < 0.05) with at least one disease, corresponding to
603 autoimmune, cardiovascular, respiratory, and neurological disorders (**Figure 7A**).

604 Of the 109 significant disease-vTR associations identified, 40 are consistent with
605 documented links between the disease and the virus encoding the vTR (**Data S7**). Several
606 studies have shown that HCMV-infected individuals have a higher prevalence of cardiovascular
607 diseases.^{106,107} For instance, HCMV IE2 promotes atherosclerosis by inhibiting cell death of

608 vascular smooth muscle cells.^{108,109} We show that genes upregulated by HCMV IE2 are
609 enriched in those associated with cardioembolic stroke and atrial fibrillation/flutter, suggesting
610 another potential mechanism (**Figure 7A**). In addition, genes dysregulated by HCMV IE1
611 overlapped with those associated with multiple neurological disorders, consistent with reports of
612 HCMV driving these diseases and the role of IE1 in perturbing neuronal development and
613 function.^{110,111} We also found several novel associations, including between DR7L (HHV-6A)
614 and chronic obstructive pulmonary disease, and between UL48 (HHV-2) and COVID-19 severity
615 (**Figure 7A**). These results suggest that vTRs extensively reprogram host transcriptional
616 networks, positioning them as potential intermediaries that connect genetic risk variants to
617 disease-related gene dysregulation.

618 The disease risk genes affected generally vary across different vTRs, even those from
619 the same virus (**Figure 7B**). However, a few disease genes are frequently targeted by multiple
620 vTRs. Many of these genes encode immune regulators (e.g., *HLA-A/B/C/DQB1*, *MICA*, *TAP2*,
621 *TNF*) or components of signaling and chromatin-modifying complexes (e.g., *MED13*, *MED19*,
622 *PBRM1*, *KANSL1*, *GATAD2A*), while others are metabolic genes (e.g., *FADS1/2*). The recurrent
623 modulation of these loci by multiple vTRs suggests that viral infection may amplify or unmask
624 the effects of genetic variants at these sites, thereby influencing disease penetrance or severity.

625 To determine whether the associations between vTRs and disease loci could be
626 mediated by human regulatory factors, we integrated vTR–disease associations with
627 hTF/cofactors CHIP-seq binding at GWAS loci for vTRs and hTFs/cofactors known to interact by
628 PPIs. We detected 11 significant vTR–hTF/cofactor–disease trios (**Data S8**), including several
629 involving hypothyroidism or rheumatoid arthritis, and Parkinson’s disease. Many of these trios
630 contained overlapping SNPs between the vTR-associated loci and hTF/CoF binding sites
631 (**Figure 7C**). For instance, vIRF-3 (KSHV) dysregulates the expression of several genes in
632 proximity of Parkinson’s disease risk loci which also show recruitment of MYC and EP300, two
633 proteins reported to interact with vIRF-3. Together, these results suggest that some vTR effects

634 at disease loci may be mediated through vTR recruitment by human transcriptional regulators
635 as has been reported for EBNA2 and RBPJ. ^{18,103,104,105}

636

637 **Discussion**

638 We systematically examined 95 vTRs across diverse human viruses, assessing their effects on
639 transcription, DNA binding, transcriptional activity, and PPIs, providing a framework to
640 understand how these proteins rewire host cellular programs and contribute to viral replication,
641 persistence, and pathogenesis. For instance, we observe that vTRs across viruses consistently
642 perturb host pathways involved in proliferation, metabolism, DNA damage, and immune
643 response, all of which contribute to viral replication and survival. This illustrates how vTRs act
644 as powerful modulators of host cell states, enabling viruses to simultaneously influence multiple
645 host pathways and drive broad shifts in cellular behavior.

646 vTRs use different mechanisms to target these pathways. Although in some cases this is
647 achieved by direct binding to DNA, in most cases the transcriptional effects are likely driven by
648 hijacking endogenous regulatory proteins. One mechanism involves indirect recruitment by
649 tethering to hTFs, consistent with findings that vTR ChIP-seq peaks are enriched for binding
650 sites of hTFs that physically interact with the vTR.^{6,18,20} In other cases, vTRs cooperate with
651 hTFs, which could re-direct hTFs to other genomic locations or change their activity (e.g., IRF1-
652 E7). A less explored strategy involves vTRs preventing the binding of hTFs that regulate cellular
653 programs that interfere with viral replication (e.g., HPV E7 antagonizing E2F4). Together, these
654 strategies enable vTRs to rewire existing transcriptional programs that control specific biological
655 processes, which is more parsimonious than creating entirely new programs through vTR
656 binding recruitment to multiple loci. Interestingly, some vTRs function through multiple
657 mechanisms (e.g., directly binding to DNA, cooperating with hTFs, and antagonizing other
658 hTFs), which could be leveraged by viruses with compact genomes to rewire diverse pathways
659 using few vTRs.

660 Many vTRs are multifunctional proteins that can affect host pathways through a variety
661 of mechanisms, such as targeted degradation or signaling inhibition. For example, in addition to
662 exhibiting potentially direct and cooperative DNA binding, antagonism of hTFs, and intrinsic
663 transcriptional activity, HPV E6 promotes p53 degradation, whereas HPV E7 promotes the
664 degradation of RB1.^{112,113} Thus, some of the transcriptional signatures we observe are likely a
665 combination of direct transcriptional and indirect effects. Further, viruses also encode proteins
666 that disrupt host pathways independently of transcriptional control. These include factors that
667 promote protein degradation (e.g., KSHV K3 and K5), mimic host molecules (e.g., HCMV US28,
668 HIV-1 Gp120), or scaffold host signaling complexes (e.g., HHV-1/2 UL46).^{114–116} Therefore,
669 vTRs may buffer, enhance, or act orthogonally to these signaling modulators within multi-
670 layered regulatory systems.

671 We found that vTRs from the same virus can have both overlapping and distinct roles in
672 modulating host pathways. Although viruses have compact genomes with relatively few protein-
673 coding genes, they may preserve functional redundancy for several reasons. Redundant vTRs
674 can provide continuity in host regulation across different stages of infection (e.g., early and late
675 vTRs both suppress immune pathways) or serve as a failsafe to counteract antiviral defenses
676 that disable individual proteins. vTRs can also exhibit a division of labor, either by targeting
677 different pathways that affect the various processes needed for viral replication or persistence,
678 targeting parallel pathways that converge on the same cellular process, or by having opposing
679 effects on the same pathway depending on context. These patterns suggest that redundancy
680 and specialization among vTRs constitute complementary strategies that enable viruses to exert
681 robust and fine-tuned control over their environment.

682 vTRs from unrelated viral species with no structural homology can produce strikingly
683 similar effects on host pathways, underscoring widespread selective pressure to target
684 conserved ‘pressure points’ in host biology. Conversely, homologous vTRs from closely related
685 viruses often differ in function and mechanism. While broad regulatory agreement is shaped by

686 the fundamental requirements for viral replication and survival, factors such as tropism can drive
687 diversification of otherwise similar vTRs. These functional differences among homologs may
688 also contribute to differences in pathogenicity, as seen in E2/E6/E7 across low- and high-risk
689 HPVs or in the Tax proteins of HTLV-1, -2, and -3.^{117–120}

690 Our analysis uncovered widespread associations between disease risk loci and genes
691 modulated by diverse vTRs, indicating that interactions between viral activity and host genetic
692 variation may be far more pervasive than previously appreciated. Although determining
693 causality will require longitudinal cohorts, integrated viral-host genomic and transcriptomic
694 datasets, and functional studies in primary human systems, the patterns we observe suggest
695 that vTRs often modulate host regulatory networks that contribute to disease susceptibility. In
696 this framework, viral infection may act as a broad environmental trigger that functionally
697 engages susceptibility loci, influencing disease penetrance, severity, and heterogeneity. Given
698 the high prevalence of many of these viruses, these findings underscore the importance of
699 systematically incorporating viral serostatus into GWAS designs to more accurately assess the
700 combined effects of inherited and viral factors on complex disease risk.

701 Altogether, our findings highlight vTRs as versatile regulators that leverage diverse
702 molecular mechanisms yet consistently converge on core host pathways essential for
703 replication, persistence, and immune evasion. Beyond defining these principles, this work
704 establishes a broadly applicable resource for the virology community. The multi-modal datasets
705 generated will enable researchers studying a specific vTR or virus to contextualize their findings
706 within a comparative framework. Such cross-virus comparisons can reveal whether vTRs not
707 tested in our study, a newly identified vTR or a vTR ortholog from specific strains act through
708 strategies already observed in our datasets. This may suggest candidate host proteins,
709 pathways, mechanisms of DNA recruitment, or links to disease to prioritize for in-depth
710 characterization. Likewise, our multimodal profiles can help reinterpret viral infection phenotypes
711 by pointing to underlying vTR drivers. By mapping how vTRs engage host gene regulatory

712 networks, this work identifies conserved regulatory nodes that may offer new therapeutic targets
713 in both acute and chronic infections. Together, our work creates a foundation for future
714 investigations into the roles of vTRs in viral infection and disease.

715

716 **Resource availability**

717 **Lead contact**

718 Requests for information should be directed to Juan I. Fuxman Bass (fuxman@bu.edu).

719

720 **Materials availability**

721 All unique/stable reagents generated in this study will be made available from the lead contact
722 with a completed material transfer agreement.

723

724 **Data and code availability**

725 Original code is available at <https://github.com/FuxmanBass-lab/vTRs>. Any additional
726 information required to reanalyze the data reported in this paper is available from the lead
727 contact upon request.

728

729 **Acknowledgments**

730 The work was supported by NIH grants R35GM128625 (to J.I.F.B.), R35GM133658 (to S.S.Y.),
731 R35GM137836 (to N.S.), U01CA232161 (to J.I.F.B., M.V., and M.L.B.), R01HG010730,
732 U24HG013078, R01NS099068, and R01AI024717 (to M.T.W.), and Alfred P. Sloan Scholar
733 Research Fellowship grant FG-2018-10723 (to N.S.). M.Y.E and P.T. were supported by NIH
734 training grant T32GM150533. P.D. was supported by NIH training grant T32AR069512. S.K.
735 was supported by NIH grant K99HG013675. S.R. was supported by the Little Warrior
736 Foundation and the Vilas Associate Fellowship.

737

738

739 **Author contributions**

740 Conceptualization, J.T.R., X.L., J.I.F.B. ; validation, J.T.R., X.L., L.F.S-U., B.E. ; formal analysis,
741 J.T.R., X.L., L.S-U., M.Y.E., J.E.C., P.D., B.E., G.M-E., Z.L., P.T., A.B., S.S., T.H., J.I.F.B. ;
742 investigation, J.T.R., X.L., A.B., C.S., J.E.C., R.L., B.E., Y.L., K.S-F., S.K., S.S., N.S., C.L., L.M-
743 C., J.I.F.B. ; resources, J.I.F.B., M.V., S.R., M.L.B., M.T.W., ; data curation, J.T.R., X.L., J.I.F.B.,
744 M.W.; writing – original draft, J.T.R., J.I.F.B.; writing – review and editing, J.T.R., J.I.F.B., N.S.,
745 S.Y., S.R., M.T.W., A.B., L.F.S-U., M.L.B., S.K., M.V.; visualization, J.T.R., M.Y.E., B.E., A.B.,
746 J.E.C., J.I.F.B.; supervision, J.I.F.B., S.R., M.V., M.C., M.L.B., M.T.W.; project administration,
747 J.I.F.B.; and funding acquisition, J.I.F.B, M.V., S.R., M.L.B., M.T.W.

748

749 **Declaration of interests**

750 The authors declare no competing interests.

751

752 **Figure legends**

753 **Figure 1: vTR1.0: a resource to study the viral transcriptional regulator functional** 754 **landscape**

755 (A) Schematic overview of vTR modulation of human transcription.

756 (B) Overview of multimodal interrogation of vTR function. eY1H, enhanced yeast one-hybrid;
757 pY1H, paired yeast one-hybrid; Y2H, yeast two-hybrid; M1H, mammalian one-hybrid. Gal4-AD,
758 Gal4 activation domain; Gal4-DBD, Gal4 DNA-binding domain; Gal4-UAS, Gal4 upstream
759 activation sequence; vTR, viral transcriptional regulator; hTF, human transcription factor.

760 (C) Percentage of vTRs from different viral families represented across all annotated vTRs, the
761 vTR1.0 resource, and tested in each experimental modality.

762 (D) Data acquired for each vTR across experimental modalities. Columns correspond to vTRs
763 (virus of origin in parenthesis). Rows correspond to each experimental modality. Black cells
764 indicate data generate for a given vTR in each modality (based on parameters and thresholds
765 for each experiment).

766

767 **Figure 2: Perturbation of human gene expression by vTRs**

768 (A) Aggregated results of gene set enrichment analysis from cells expressing different vTRs.
769 vTR are clustered based on CSI-corrected Pearson correlation coefficient. Rows correspond to
770 gene sets clustered based on gene similarity. Normalized enrichment scores (NES) are
771 represented for each vTR as a color gradient. The number of vTRs with a positive or negative
772 NES per pathway is indicated in grey.

773 (B) Distribution of connection specificity index (CSI) for all pairs of vTRs, vTRs from the same
774 family, vTR orthologs, and vTRs from the same virus. Solid lines denote the median and dashed
775 lines denote quartiles.

776 (C-E) Scatter plots comparing the NES of pathways dysregulated by pairs of vTRs. Number
777 lines above indicate the CSI correlation for the given pair of vTRs. Selected pathways are
778 colored. (C) Adenovirus A E1A versus IVa2. (D) HCMV IE1 versus IE2. (E) HPV-5 E2 versus
779 HCMV UL34.

780 (F) Alphafold2 models for vTRs from Cluster 2 in Figure 2A. Color indicates viral family.

781 (G) Distribution of CSI correlation scores for all vTRs in resting cells, all vTRs tested in Sendai
782 Virus-infected cells, and vTRs compared between untreated and Sendai Virus-infected cells.
783 SeV - Sendai Virus.

784 (H) Scatter plot comparing the NES of pathways dysregulated by vaccinia virus (VACV) VLTF-3
785 in untreated and Sendai Virus-infected cells.

786 (I) Heatmap of NES from GSEA comparing SeV infection versus no infection in vector and vTR
787 conditions. Pathways shown are significantly altered by SeV infection and display opposite
788 responses between vector and vTR.

789

790 **Figure 3: vTRs bind host regulatory elements and alter chromatin structure**

791 (A) Protein-DNA interactions for vTRs (left), vTRs cooperating with hTFs (right), and human
792 promoter sequences. Hexagons represent vTRs, and are colored by virus. Purple circles
793 represent hTFs. Squares represent human promoters.

794 (B) Network of relationships between hTFs and vTRs. Blue edges represent cooperativity, red
795 edges represent antagonism. Edge thickness indicates the number of promoters at which a
796 specific interaction occurs.

797 (C–F and H) Representative pY1H interactions for hTF-vTR pairs. Italicized gene names (left)
798 indicate the tested promoter bait. Yeast strains shown: empty vector control, hTF only, vTR
799 only, hTF-vTR pair. (C) Cooperativity between DDIT3 and HBZ (HTLV-1) at MYC and FGFR3
800 promoters. (D) Cooperativity between IRF3 and E6 (HPV-5) at IFNB1 promoter. Cooperativity
801 between IRF1 and E7 (HPV-5) at IFNL1, IL15, and TNFSF10 promoters. (E) Cooperativity
802 between ZNF398 and E7 (HPV-16) at ACSL6 promoter. (F) Antagonism of E2F4 by multiple E7
803 homologs at the IL7 promoter. (H) Antagonism of ZNF281 by IE2 (HCMV) at KLK2 and ID3
804 promoters; cooperativity between ZNF281 and IE2 at IL1B promoter.

805 (G) AlphaFold3 models of interactions between E2F4 and E7 from different HPV strains.

806 (I) Heatmap of NES scores for Interleukin pathways derived from BRB-seq data for IE2 (HCMV)
807 in SeV-infected and uninfected cells.

808 (J) vTR DNA binding modalities described in this manuscript (light blue), reported in the
809 literature (green), or both (purple).

810 (K) Heatmap of z-score normalized chromatin accessibility at 19,785 peaks that are differentially
811 accessible ($FDR \leq 0.1$ and $\log_2FC \geq 1$) in at least one vTR surveyed via PROD-ATAC comparing
812 E4ORF6/7 (Adv B), HBx (HBV), EBNA3A (EBV), and EBNA3B (EBV). Columns of peaks are
813 hierarchically clustered.

814 (L-M) Representative DNA motif enrichment within increased/decreased differentially accessible
815 peaks for EBV EBNA3A (L) and Adenovirus B E4ORF6/7 (M). Displayed values were calculated
816 using hypergeometric tests and plotted relative to the ranked order of all queried motifs.

817

818 **Figure 4: vTRs display intrinsic transcription activity and interact with host regulators**

819 (A) Distribution of transcriptional activities elicited by hTFs and vTRs by M1H assays using a
820 minimal promoter. Significance determined by two-tailed Mann-Whitney test.

821 (B) Transcriptional activities of vTRs across viral families by M1H assays with a moderate
822 promoter. Red and blue points indicate activating ($L2FC \geq 1$) and repressing ($L2FC \leq -1$) vTRs,
823 respectively.

824 (C) Distribution of transcriptional activities for vTRs expressed at different timepoints of
825 infection. IE, immediate early; E, early; E/L, early/late; L, late; Lat, latent. Distributions were
826 compared using One-Way ANOVA. Asterisks correspond to multiple comparisons adjusted p-
827 values (*** $P < 0.001$).

828 (D) Protein-protein interaction (PPI) network curated from HVIDB (<http://zzdlab.com/hvidb>) and
829 the Y2H screen. Hexagons indicate vTRs and circles indicate human proteins. Edges indicate
830 the source of the PPI. hTF, human transcription factor; CoF, cofactor.

831 (E) Proportion of PPIs between viral proteins, vTRs, or hTFs and hTFs, cofactors (CoF),
832 signaling proteins, or other proteins. * $p < 0.01$ by two-tailed proportion comparison test.

833 (F) PPI Sub-network between 8 vTRs and TLE5.

834 (G) Western blot showing co-immunoprecipitation of TLE5 with FLAG-tagged HHV2 US1 and
835 HCMV UL82.

836 (H) Alphafold3 model of interactions between TLE5 and HHV2 US1 and HCMV UL82.

837 (I) Proportion of PPIs between vTRs and hTFs, CoFs or other proteins. Only vTRs with at least
838 3 human PPIs are shown.

839 (J) PPI log2fold enrichment between vTRs expressed at different timepoints of infection for ten
840 categories of human proteins.

841 (K) Percentage of vTRs or hTFs with PPIs with individual human proteins. Interactions shown
842 are the union of vTR1.0 Y2H, HuRI (<http://www.interactome-atlas.org>), HVIDB, and BioGRID.
843 Magenta dots indicate human proteins preferentially interacting with hTFs, gold dots indicate
844 proteins preferentially interacting with vTRs, and cyan dots indicate proteins that frequently
845 interact with both vTRs and hTFs. Pie charts represent the fraction of different protein classes
846 within each previously described subset of proteins.

847 (L) Proportion of vTR homologs (left) or hTF paralogs (right) represented in comparisons with
848 high jaccard similarity (>0.3) or low jaccard similarity (<0.3).

849 (M) Probability density distributions of Jaccard PPI profile similarity scores within vTRs (blue),
850 within hTFs (orange), or between vTRs and hTFs (green).

851

852 **Figure 5: Functional diversity and redundancy between vTRs from the same virus**

853 (A–B) CSI correlation scores for pairs of vTRs encoded by the same virus in resting (A) and
854 SeV-infected (B) cells. For each virus, points represent within-virus vTR comparisons, shown
855 relative to the distribution of all other possible pairwise comparisons involving these vTRs.

856 (C) Distributions of CSI correlation scores for vTR pairs from the same virus with either the
857 same or different expression timing.

858 (D, F) CSI correlation score comparisons for five EBV (D) and four HCMV (F) vTRs in resting
859 cells.

860 (E, G) Heatmaps showing the number of overlapping pathways regulated by EBV vTRs (E) or
861 HCMV vTRs (G) across four functional categories. Diagonal cells indicate the total pathways
862 regulated by each vTR, and off-diagonal cells indicate the number of pathways shared between
863 vTR pairs.

864 (H) Cumulative number of pathways affected by the vTR repertoire of different viruses. Only
865 viruses with at least 3 vTRs in our dataset are shown.

866 (I) Probability density distributions of jaccard PPI profile similarity scores for vTRs from the
867 same virus (blue) or different viruses (orange). Significance determined by two-sided Mann-
868 Whitney's U-test.

869 (J) PPI networks for each virus showing human proteins that interact with at least three vTRs.
870 Hexagons indicate vTRs and circles indicate human proteins.

871

872 **Figure 6: Functional variation across vTR homologs**

873 (A) Survey of data available for sets of homologous vTRs. Cell color gradient indicates the
874 proportion of homologs in each data set. Black bars indicate the total number of vTR homologs
875 per set. BRB-, BRB-seq in resting cells; BRB+, BRB-seq in Sendai Virus-infected cells; eY1H,
876 enhanced yeast one-hybrid; pY1H, paired yeast one-hybrid; M1H, mammalian one-hybrid; Y2H,
877 yeast two-hybrid.

878 (B) CSI correlation scores for pairs of vTR homologs. Blue and yellow dots indicate
879 comparisons from uninfected or Sendai virus-infected cells.

880 (C) Comparison of up- and down-regulated Cell-Cell signaling pathways between HHV ICP22
881 homologs. Color gradient indicates the number of pathways affected in uninfected conditions.
882 Venn diagram represents the shared and distinct pathways upregulated by both US1 (HHV-2)
883 and IE63 (VZV). NES, normalized enrichment score.

884 (D) Scatter plots representing the relationship between the percent amino acid identity between
885 homologs and CSI correlation score. Left plot, uninfected cells; Right plot, infected cells.
886 Pearson r values are indicated in the plot.

887 (E) Comparison of up- and down-regulated pathways between HPV E7 homologs. Color
888 gradient indicates the number of pathways affected in uninfected conditions.

889 (F-G) Scatter plots comparing the NES of pathways dysregulated by HPV-16 E2 (F) and HPV-5
890 E2 (G) in uninfected versus Sendai Virus-infected conditions. Selected pathways are colored.
891 Number lines indicate the CSI correlation score for the given E2 homolog in uninfected versus
892 SeV-infected cells.

893 (H) CSI correlation scores for vTR homologs in uninfected versus SeV-infected cells.

894 (I) Transcriptional activities of vTRs across homolog groups via M1H assays using a moderate
895 promoter. Red and blue points indicate activating ($L2FC \geq 1$) and repressing ($L2FC \leq -1$) vTRs,
896 respectively.

897 (J-K) PPIs (left) and M1H activity (right) for two Adenovirus E2A (J) and four HPV E6 (K) and
898 homologs.

899 (L) Heatmap of z-score normalized chromatin accessibility at 4,656 peaks that are differentially
900 accessible ($FDR \leq 0.1$ and $\log_2FC \geq 1$) via PROD-ATAC comparing E4ORF6/7 homologs
901 from five Adenoviruses. Peak columns are hierarchically clustered.

902 (M) Representative DNA motif enrichment within increased differentially accessible peaks for
903 four Adv E4ORF6/7 homologs. Displayed values were calculated using hypergeometric tests
904 and plotted relative to the ranked order of all queried motifs.

905

906 **Figure 7: Association between vTRs and disease**

907 (A) Fold enrichment of disease risk loci that overlap with genes up- or down-regulated by the
908 expression of different vTRs (gene transcription start site +/- 1 kb). Only associations with an

909 FDR < 0.05 are shown. Asterisks indicate cases where the virus expressing a particular vTR
910 has been associated with the corresponding disease in the literature.

911 (B) Network connecting vTRs and differentially expressed genes that are associated with
912 disease risk loci. Edge width indicates the number of diseases in which the gene was
913 significantly associated. Human gene node size corresponds to the number of vTRs that
914 dysregulate the expression of the gene. Genes dysregulated by 5 or more vTRs are labeled.

915 (C) Network showing significant vTR–hTF/CoF–GWAS locus trios for Hypothyroidism or
916 rheumatoid arthritis, and Parkinson’s disease. Edges represent overlap between vTR DEGs and
917 the disease risk SNP, and between ChIP-seq peaks for the hTF/CoF and the same disease risk
918 SNP, for pairs of vTRs and hTFs/CoFs with reported PPIs.

919

920 **Supplementary Figures**

921 **Figure S1: Overview of datasets generated using vTR1.0**

922 (A) Number of differentially expressed genes for each vTR successfully tested via BRB-seq.
923 Each point represents the number of up- and down-regulated genes driven by the expression of
924 each vTR ($|\text{Log}_2 \text{FC}| \geq 0.5$ and $p \leq 0.05$).

925 (B) Proportion of protein-DNA interactions (PDIs) determined for vTRs tested using eY1H and
926 pY1H assays that were classified as independent (does not require a partner), cooperative
927 (binding is enhanced by a partner), antagonistic (one protein prevents the binding of the other),
928 or complex (binding modality depends on the target sequence).

929 (C) Histogram of distribution of transcriptional activity for vTRs tested using M1H assays,
930 relative to vector control. Activators ($\text{Log}_2 \text{FC} \geq 1$) are colored red and repressors ($\text{Log}_2 \text{FC} \leq -$
931 1) are colored blue.

932 (D) Distribution of protein-protein interactions (PPIs) detected between vTRs and human
933 proteins using Y2H assays.

934

935 **Figure S2: Alphafold3 models between vTRs and hTFs**

936 Alphafold3 models of vTRs-hTF pairs where the vTR antagonizes the binding of a hTF to DNA.
937 vTR is shown in red, the hTF DBD is shown in blue, and non-DNA regions are shown in gray.

938

939 **Figure S3: pY1H antagonistic interactions between ZNF281 and IE2 (HCMV)**

940 Antagonistic pY1H interactions involving IE2 (HCMV) and hTF ZNF281. Italicized gene names
941 indicate the promoter tested. Yeast strains shown: empty vector control, ZNF281 only, IE2 only,
942 and ZNF281-IE2 pair.

943

944 **Figure S4: Differentially accessible chromatin regions identified by PROD-ATAC**

945 (A) Volcano plots depicting the $-\log(\text{FDR})$ versus $\log_2\text{FC}$ for each called peak comparing
946 pseudobulk replicates of the corresponding vTR to the Empty Vector control. Peaks with
947 increased accessibility ($\text{FDR} \leq 0.1$ and $\log_2\text{FC} \geq 1$) are red, and peaks with decreased
948 accessibility ($\text{FDR} \leq 0.1$ and $\log_2\text{FC} \leq -1$) are blue.

949 (B) Number of differentially expressed genes driven by expression of E4ORF6/7 from different
950 adenoviruses.

951

952

953 **Methods**

954 **EXPERIMENTAL APPROACHES**

955 **Generation of vTR1.0 entry clone collection**

956 95 vTR ORF sequences (**Data S1**) were synthesized as gene fragments (Twist Bioscience) and
957 subsequently cloned into pDONR221 by Gateway BP reaction (Thermo Fisher Scientific)
958 followed by transformation into *E. coli* DH5 α . Transformed *E. coli* were then plated onto LB agar
959 containing 50 $\mu\text{g}/\text{mL}$ Kanamycin overnight at 37 C. Colonies for each transformation were
960 confirmed by Sanger sequencing and expanded to generate our vTR entry clone collection.

961

962 **BRB-seq experiments**

963 To determine the transcriptomic effects of vTRs in human cells, we performed bulk RNA
964 barcoding and sequencing (BRB-seq) in HEK293T cells expressing individual vTRs. Expression
965 vTR clones were generated via Gateway LR cloning into the pEZY3 constitutive expression
966 vector (Addgene plasmid #18672). Following transformation, plasmids were extracted, and
967 insertion was confirmed via PCR and gel electrophoresis. The full list of vTRs tested by BRB-
968 seq is provided in **Data S2**.

969 For BRB-seq experiments, HEK293T cells were cultured in DMEM media supplemented
970 with 10% FBS and seeded in two 96-well plates at a density of 18,000 cells/well. The following
971 day, cells were transfected in quadruplicate using Lipofectamine 3000 (Thermo Fisher
972 Scientific) with 80 ng of the pEZY3-vTR plasmids, as well as empty pEZY3 vector controls. After
973 24 hours, cells were either infected with 4.0×10^6 CEID₅₀/mL Sendai virus (VR-907, ATCC), or
974 left uninfected. RNAs were harvested 2 days post-transfection, a time point that we showed has
975 minimal interferon pathway activation due to transfection. Sequencing libraries were prepared
976 using the MERCURIUS DRUG-seq kit (Alithea Genomics) according to manufacturer's
977 instructions and as described previously.²⁴ Briefly, HEK293T cells were permeabilized using a
978 cell lysis buffer on ice 15 min with periodic agitation, followed by centrifugation to clear cellular
979 debris. Individual RNA-containing lysates were then reverse-transcribed using barcoded oligo-
980 dT primers such that the resulting cDNA from each individual sample was uniquely barcode-
981 labeled. cDNA from all samples in a single plate were then pooled and purified using the
982 column-based Zymo Clean & Concentration Kit according to manufacturer's instructions (Zymo,
983 D4014). The pooled cDNA was then cleared of non-incorporated primers via exonuclease
984 digestion, followed by second strand synthesis and quantification of ds-cDNA via Qubit HS-DNA
985 kit (Thermo Fisher). Tagmentation was then performed on 20 ng cDNA, followed by library

986 indexing and amplification using standard Illumina NGS adapter sequences. Indexed libraries
987 were sequenced at a depth of 5 million raw reads per sample on an Illumina Novaseq platform.

988

989 **Enhanced yeast one-hybrid (eY1H) assay**

990 To detect PDIs between vTRs and cytokine gene promoters, eY1H assays were performed as
991 previously described.¹²¹⁻¹²³ vTRs prey clones were generated via Gateway LR into pDEST-
992 AD2 μ (Walhout lab) such that each vTR was fused with the yeast Gal4 Activation Domain. vTR-
993 prey strains were generated via transformation into Y \square 1867 yeast as previously described.^{121,124}
994 Yeast were inoculated in 1 L liquid YAPD media at a concentration of OD600 = 0.15 and
995 incubated at 30°C shaking at 200 rpm until they reached OD600 = 0.4-0.6, washed with sterile
996 water, and washed again with TE + 0.1 M lithium acetate (TE/LiAc). Yeast were resuspended in
997 TE/LiAc with salmon sperm DNA (ThermoFisher #15632011) at a dilution of 1:10 before adding
998 250 ng of the vTR clone. Six volumes of TE/LiAc + 40% polyethylene glycol were then added,
999 and samples were mixed gently ten times. Yeast were then incubated at 30°C without shaking
1000 for 30 minutes followed by 42°C for 20 min, then resuspended in sterile water. Transformed
1001 yeast were plated in selective media lacking tryptophan to select for transformants. vTR prey
1002 yeast strains were confirmed by Sanger sequencing.

1003 DNA-bait strains corresponding to 112 human cytokine promoters were previously
1004 generated using the Y1HaS2 yeast strain.²⁵ Bait-strains carry two integrated copies of the
1005 promoter element upstream of HIS3, which allows yeast to grow in the absence of histidine and
1006 overcome growth inhibition by 3-amino-1, 2, 4-triazole (3AT), and LacZ which causes yeast
1007 colonies to turn blue in the presence of 5-bromo-4-chloro-3-indolyl-beta-D-galacto-pyranoside
1008 (X-gal).

1009 eY1H was performed as previously described¹²¹⁻¹²³ using a high-density array ROTOR
1010 robotic platform (Singer Instruments). The vTR yeast array and cytokine promoter yeast strains
1011 were mated pairwise and spotted on permissive agar media for 1 day at 30°C followed by

1012 selection on agar plates lacking Uracil and Tryptophan for 2 days to select diploid yeast.
1013 Selected diploid yeast were then transferred to selective media agar plates lacking uracil,
1014 tryptophan, and histidine, with 5mM 3AT and 320 mg/L X-gal. These readout plates were
1015 imaged at 2-, 3-, 4-, and 7-days post-plating. Interactions were tested in quadruplicate and were
1016 manually curated by 2 researchers. Only vTR-promoter pairs that resulted in growth and blue
1017 color for at least two of the four colonies were considered positive (**Data S3**). At least 90% of
1018 interactions were detected with all four colonies.

1019

1020 **Paired Yeast one-hybrid (pY1H) assay**

1021 To detect cooperative binding and antagonism between vTRs and hTFs, pY1H assays were
1022 performed as previously described.²⁶ Prey strains expressing 113 vTR-hTF pairs were
1023 generated using a Y□1867 strain where the LEU2 gene had been disrupted (Y□1867Δleu2) to
1024 accommodate transformation with plasmids containing both TRP1 and LEU2 selection
1025 markers.²⁶ This array vTR-hTF array also included clones with single vTRs or hTFs expressed.
1026 DNA-bait strains corresponding to 39 human cytokine promoters and 83 cancer-related gene
1027 promoters were previously generated using the Y1HaS2 yeast strain.^{25,125}

1028 pY1H was performed using a high-density array ROTOR robotic platform (Singer
1029 Instruments) as previously described.²⁶ Briefly, the vTR-hTF yeast array and human promoter
1030 yeast strains were mated pairwise (in quadruplicate) on permissive medium agar plates and
1031 incubated at 30°C for 1 d. Mated yeast were then transferred to selective medium agar plates
1032 lacking uracil, leucine, and tryptophan to select for successfully mated yeast and incubated at
1033 30°C for 2 d. These selection plates were imaged and analyzed to identify array locations with
1034 failed yeast growth, which were then removed from further analysis. Diploid yeast were finally
1035 transferred to selective medium agar plates lacking uracil, leucine, tryptophan, and histidine,
1036 with 5 mM 3AT and 320 mg/liter X-gal. These Readout plates were imaged 2, 3, 4, and 7 d after
1037 final plating.

1038 Yeast plate images were processed and visualized using DISHA (Detection of
1039 Interactions Software for High-throughput Analyses) software.²⁶ vTR-hTF pair strains were
1040 sorted based on each index (cooperativity, antagonism index 1, and antagonism index 2)
1041 separately. Images were then manually analyzed to identify cooperative and antagonistic
1042 interactions. To call an interaction, the following criteria was used: 1) vTR-hTF pair, vTR, and
1043 hTF yeast strains all showed growth in the mating selection plates before transfer to readout
1044 plates; and 2) on readout plates, ≥ 3 out of 4 replicate colonies were uniform for vTR-hTF pair,
1045 vTR, and hTF yeast strains. For cooperative interactions, vTR-hTF pair yeast showed a strong
1046 or moderate reporter activity relative to the empty-empty strain, and vTR and hTF yeast showed
1047 no or only weak reporter activity. For antagonistic interactions, vTR and/or hTF yeast showed a
1048 strong or moderate reporter activity relative to the empty-empty strain and the vTR-hTF pair
1049 yeast showed no or only weak reporter activity. Cooperative and antagonistic interactions are
1050 provided in **Data S4**.

1051

1052 **Mammalian one-hybrid (M1H) assays**

1053 To measure vTR transcriptional activity, M1H assays were performed in HEK293T cells.^{75,125} In
1054 this assay, vTR fused to the Gal4 DNA-binding domain are recruited to the upstream activating
1055 sequence (UAS) upstream of the firefly luciferase gene. Changes in expression of firefly
1056 luciferase are reflective of the endogenous activating or repressing activity of the vTR.

1057 vTRs were cloned into the DB-pEZY3 vector via Gateway LR such that the vTRs were
1058 N-terminally fused to Gal4 DNA-binding domain.¹²⁶ M1H assays were performed using pGL4.23
1059 luciferase reporter constructs. For low-background M1H assays, a 4xUAS + minimal promoter
1060 construct was used, as described.^{75,125} We also performed M1H assays using a moderate
1061 background activity construct containing 4xUAS + moderate promoter containing the Syn2B10

1062 enhancer sequence previously described¹²⁶ to detect transcriptional repression with higher
1063 sensitivity, as well as activation.

1064 HEK293T cells were cultured in DMEM media supplemented with 10% FBS and plated
1065 in 96-well white opaque plates (Corning) at a density of 10,000 cells/well and incubated at 37°C,
1066 5% CO₂ for one day. Cells were then transfected with 80 ng of vTR (DB-pEZY3) plasmid, 20 ng
1067 4xUAS construct, and 10 ng of renilla luciferase plasmid as a transfection normalization control.
1068 An empty DB-pEZY3 plasmid and 4xUAS construct plasmid were co-transfected to serve as a
1069 negative control. Cells were incubated for 2 days after transfection at 37C with 5% CO₂,
1070 followed by measurement of both firefly and renilla luciferase activity using the Dual-Glo
1071 Luciferase Assay System (Promega). Non-transfected cells were used to subtract background
1072 for firefly/renilla luciferase activities. Firefly luciferase activity was then normalized with renilla
1073 luciferase activity in each well. vTR activities using both reporter systems are provided in **Data**
1074 **S5**.

1075

1076 **PROD-ATAC Pooled Library Generation**

1077 The pooled library of HEK293T cells used to generate PROD-ATAC (Protein-Coding single-cell
1078 Assay for Transposase Accessible Chromatin) chromatin accessibility profiles were produced
1079 for the described set of vTR sequences as previously described in detail (Frenkel et al, 2024).
1080 Briefly, 3-wells of a 6-well plate were seeded with 400,000 HEK293T-B4 attP-containing landing
1081 pad cells and left to attach overnight in DMEM media supplemented with 10% FBS. At
1082 approximately ~50% confluency, each well was transfected (using Lipofectamine 3000 in Opti-
1083 MEM) with 1,500 ng donor attB library, encoding each of the relevant vTR sequences, and 100
1084 ng of pCAG-NLS-HA-Bxb1 (Addgene, 51271). Liposome-containing media was aspirated 18
1085 hours post-transfection and replaced with fresh complete media containing 0.8 ug/ml puromycin.
1086 After 3 days of puromycin selection, the 3-wells were pooled into a single T-25 flask. Passages
1087 were subsequently performed every 2 days (when cells reached ~70% confluency). At 12 days

1088 post-selection start, several cell aliquots were frozen (5% DMSO v/v) and stored in the vapor
1089 phase of a liquid nitrogen dewar.

1090

1091 **PROD-ATAC Screening**

1092 In preparation for the PROD-ATAC sequencing run, the HEK293T cell library encoding the
1093 described vTR sequences was seeded and allowed to attach overnight in DMEM media
1094 supplemented with 10% FBS. Cells were treated with 2 ug/ml doxycycline to induce library
1095 expression for 96 hours, with a single split performed at 48 hours post-induction. After this point,
1096 the PROD-ATAC single cell sequencing library generation procedure was performed as
1097 previously described using 10x Genomics scATAC kits with v2 Chemistry, with solely two
1098 deviations: 15,000 nuclei (rather than 10,000) were targeted for capture per 10x chip lane, and 8
1099 total lanes were used in the assay.¹²⁷

1100

1101 **Yeast two-hybrid (Y2H) assays**

1102 Y2H assays were performed as previously described.^{75,128} vTRs were cloned into pDESTDB-X
1103 vectors via Gateway LR such that each vTR was fused to the yeast Gal4 DNA-binding domain
1104 (DB). The competent yeast strain Y8930 (MAT α) was transformed with individual DB-vTR
1105 constructs and plated on yeast synthetic media lacking leucine to select for DB-vTR plasmid-
1106 containing yeast. Haploid DB-vTR yeast strains were tested for auto-activation of the
1107 GAL1::HIS3 reporter gene. Individual DB-vTR yeast strains were spotted on SC-Leu-His+1mM
1108 3AT media and any strains showing growth were considered auto-activators (AAs) and removed
1109 from the collection of strains to be screened.

1110 A primary Y2H screen was performed in which all non-AA vTR strains were tested
1111 against the hORFeome v9.1 collection of 17,472 ORF clones¹²⁸ tagged with Gal4 activation
1112 domain (AD). DB-vTR strains were mated individually against 99 pools of ~188 AD-ORF strains
1113 (preys). To perform the mating, fresh overnight cultures of DB-vTR strains were mixed with AD-

1114 ORF strain pools and grown overnight at 30°C in liquid rich media (YEED). After overnight
1115 growth, the mated yeast cells were transferred into liquid SC-Leu-Trp media to select for
1116 diploids and again grown overnight at 30°C. Finally, the yeast cells were spotted onto SC-Leu-
1117 Trp-His+1mM 3AT solid media to select for activation of the GAL1::HIS3 reporter gene. In
1118 parallel, diploid yeast cells were transferred onto SC-Leu-His+1mM 3AT solid media
1119 supplemented with 1 mg/l cycloheximide to test for spontaneous DB-ORF auto-activators. After
1120 72 hours incubation at 30°C, yeast that grew on SC-Leu-Trp-His+1mM 3AT but not SC-Leu-
1121 His+1mM 3AT+ 1 mg/L cycloheximide media were picked into SC-Leu-Trp grown overnight then
1122 processes to determine identity of interaction partners by Sanger sequencing. In total, 674 PPIs
1123 between vTRs and human proteins were identified, involving 41 vTRs.

1124 Following this first-pass screening, vTRs were tested pairwise for interactions with the
1125 candidate human ORFs identified in the first-pass screening in a matrix format (the 41 vTRs
1126 against the union of all ORF interactors). Yeast strains corresponding to the identified human
1127 interaction partners were picked from archival glycerol stocks, cultured in liquid medium and
1128 mated one-by-one against all 41 vTRs, processed as described above and then scored. Briefly,
1129 interactors were inoculated in 200 µL of selective media and mated overnight at 30°C in 150 µL
1130 liquid rich media (YEED). The following day, mated yeast cells were transferred to 150 µL liquid
1131 SC-Leu-Trp media to select for diploids. After overnight incubation at 30°C, 5 µL diploid yeast
1132 cells were spotted onto SC-Leu-Trp-His+1mM 3AT solid media to select for activation of the
1133 GAL1::HIS3 reporter gene as well as on SC-Leu-Trp to control for successful mating. AA tests
1134 were included by mating each Y8930:DB-ORF against a Y8800:AD-null (containing no ORF),
1135 which was included on each test plate for each individual Y8930:DB-ORF. Spots were scored
1136 for growth with scores of 0, 1, 2, 3, 4, and NA for cases where the spotting had failed. Growth
1137 scores of 0 and 1 were considered not growing. If a spot corresponding to either the pair or the
1138 corresponding AA-test did not grow on SC-Leu-Trp, the pair was scored NA. If the AA-test had a
1139 growth score of 4, the corresponding pair was scored NA. Interactions were scored positive if

1140 they had higher growth scores on SC-Leu-Trp-His+1mM 3AT solid media compared to the auto-
1141 activator test and had a growth score of at least 2; otherwise they were scored negative. All
1142 positive scored colonies were picked, lysed and the identity of the two interacting proteins was
1143 confirmed by sequencing. 86 PPIs were validated, involved in 28 vTRs.

1144 Next, we curated PPIs between non-AA vTRs and human proteins previously reported in
1145 Uniprot. All human proteins that interacted with at least one vTR, with available clones in the
1146 ORFeome, were pairwise tested against the non-AA vTRs. This led to 46 interactions, which
1147 were combined with the previous 86 PPIs for a total of 132 interactions between 33 vTRs and
1148 67 human proteins (**Data S6**).

1149

1150 **Immunoprecipitation and immunoblotting analyses.**

1151 HEK293T cells stably expressing the corresponding vTRs were lysed with RIPA lysis buffer
1152 (20mM Tris-HCl, 37mM NaCl₂, 2mM EDTA, 1% Triton-X, 10% glycerol, 0.1% SDS and 0.5%
1153 sodium deoxycholate) with protease and phosphatase inhibitors (Roche). Protein samples were
1154 quantified (Pierce BCA Protein Assay Kit, Thermo Fisher Scientific) and the same amount of
1155 cell lysates from vTR overexpressing stable cells and GFP vector control cells were incubated
1156 with an anti-Flag M2 Affinity Gel (Sigma) overnight at 4°C. The beads were washed 3x with
1157 TBST buffer and then boiled in sample buffer. The supernatants were subjected to SDS
1158 polyacrylamide gel electrophoresis and transferred to polyvinylidene difluoride membranes.
1159 Membranes were incubated with primary antibodies, including anti-AES (1:1,000; Proteintech)
1160 and anti-Flag (1:2,000; Sigma) and subsequent secondary antibody: horseradish peroxidase-
1161 conjugated Affinipure Goat Anti-Rabbit IgG(H+L) (1:3,000; Proteintech, catalog no. SA00001-2).

1162

1163 **QUANTIFICATION AND STATISTICAL ANALYSES**

1164 **BRB-seq sequence alignment**

1165 BRB-seq reads were aligned to a custom human reference based on GRCh38 (primary
1166 assembly) with Gencode v46 annotations,¹²⁹ augmented by a concatenated FASTA of all VTR
1167 sequences and a merged GTF that combined genome and VTR features. Genome indices were
1168 built with STAR v2.7.9a¹³⁰ using splice junctions (`--sjdbGTFfile Gencode+VTR, --sjdbOverhang`
1169 `79`). Alignment and counting were performed with STARsolo in CB/UMI simple mode to recover
1170 per-barcode gene counts (`--soloType CB_UMI_Simple; --soloFeatures Gene; --soloStrand`
1171 `Forward; --clipAdapterType CellRanger4; --outSAMtype BAM SortedByCoordinate; --`
1172 `outSAMunmapped Within; --outReadsUnmapped Fastx`). Barcodes and UMIs were parsed with
1173 a 14-nt cell barcode and 14-nt UMI (`--soloCBstart 1 --soloCBlen 14; --soloUMIstart 15 --`
1174 `soloUMIlen 14`), matched to a provided whitelist allowing one mismatch (`--soloCBmatchWLtype`
1175 `1MM`), and deduplicated with directional one-mismatch UMI collapsing (`--soloUMIldedup`
1176 `1MM_Directional`). STAR output included comprehensive SAM attributes (NH HI AS nM CR CY
1177 UR UY CB UB GX GN sS sQ sM).

1178

1179 **Pre-processing, Differential Expression and Pathways Analysis**

1180 Raw STARsolo matrices were imported into Seurat¹³¹ for each plate-condition, and well-level
1181 metadata were joined from barcode annotation tables. For each well, we quantified the
1182 proportion of reads mapping to the expected vTR and compared it with the most abundant vTR
1183 signal within the full vTR panel. Wells with at least 85% of reads assigned to a single vTR were
1184 flagged as highly specific and used to assess concordance with the expected assignment. For
1185 downstream analyses, we applied the following filters: (i) vTR wells were required to have at
1186 least 85% of their vTR-panel reads assigned to the expected construct and a minimum of
1187 500,000 total mapped reads; (ii) control and vector wells were required to show no dominant
1188 vTR signal (top VTR <0.01% of total reads) and at least 500,000 total mapped reads. After
1189 filtering, counts were merged across wells and joined to Gencode v46 annotations.¹²⁹ We
1190 retained protein-coding, T-cell receptor, and immunoglobulin genes, while excluding

1191 mitochondrial and ribosomal genes as well as lowly expressed genes. Normalization and
1192 differential expression were performed using DESeq2,¹³² with the vector set as the reference. A
1193 pooled matrix design that included batch as a covariate was chosen, as it showed high
1194 correlation between replicates while effectively reducing noise and confounding effects. Results
1195 were extracted using Benjamini–Hochberg correction (FDR < 0.1) without independent filtering.
1196 Gene Set Enrichment Analysis (GSEA)¹³³ used msigdb to retrieve MSigDB C2:CP-
1197 REACTOME sets¹³⁴ and was run with 10,000 permutations, Benjamini-Hochberg correction,
1198 eps=0, minGSSize=15, maxGSSize=500, and p-value cutoff reporting at 1. Pathways with a p-
1199 value > 0.05 were considered not significant.

1200

1201 **Reactome Pathway Categorization**

1202 Individual reactome pathways from BRB-seq experiments were designated under any number
1203 of the following categories: cell-cell signaling, signal transduction, immune, metabolism, stress,
1204 DNA damage repair, cell cycle, gene regulation/RNA biogenesis. Pathways were categorized
1205 based on reactome pathway descriptions (<https://reactome.org/>) and genes present in the
1206 pathway.

1207

1208 **CSI correlation calculation**

1209 To quantify sample-sample similarity at the pathway level, we constructed a matrix of
1210 normalized enrichment scores (NES) from GSEA Reactome results, setting values to zero when
1211 the corresponding pathway had a non-significant enrichment ($p > 0.05$). Pathways represented
1212 in fewer than three samples were excluded, and missing values were imputed as zero. Pairwise
1213 sample correlations were then computed using Pearson's correlation across the filtered NES
1214 matrix, and the resulting correlation distances were used as input for Connection Specificity
1215 Index (CSI).^{31,32} For each sample pair (A, B), the CSI was defined as the proportion of third
1216 samples (X) for which the maximum of the distances (A–X, B–X) was smaller than the distance

1217 between A and B. This procedure was parallelized across all sample pairs, producing a
1218 symmetric CSI matrix, which was normalized by the number of possible third samples ($n - 2$) to
1219 yield values between 0 (no concordance) and 1 (high concordance). The resulting CSI matrix
1220 was then used for downstream clustering and comparative analyses.

1221

1222 **Alphafold3 of vTR structures**

1223 Predicted three-dimensional structures of proteins were generated using AlphaFold3.¹³⁵
1224 Structural predictions were run through the publicly accessible AlphaFold3 interface using
1225 default parameters. Briefly, amino-acid sequences of each protein of interest were retrieved
1226 from UniProt and supplied as input to the AlphaFold3 prediction pipeline. Five structural models
1227 were produced per sequence. Predicted Local Distance Difference Test (pLDDT) scores and
1228 Predicted Aligned Error (PAE) heatmaps were used to assess overall model quality and to
1229 identify well-resolved regions suitable for interpretation. The highest-confidence monomer
1230 model was selected for downstream analysis and visualization, which was performed using
1231 UCSF ChimeraX.¹³⁶

1232 Protein–protein complex (heterodimer) structures were predicted using AlphaFold3's
1233 multimer mode. Human transcription factors or TLE5 were paired with vTRs and supplied jointly
1234 as separate chains in a single multimer prediction run. Five multimer models were generated for
1235 each input pair and ranked using pLDDT, inter-chain PAE, and AlphaFold3's interface
1236 confidence metrics (iPTM and chain-pair interface scores). The top-ranked multimer model was
1237 selected for downstream interpretation, and all structural visualization and interaction inspection
1238 were performed using UCSF ChimeraX.¹³⁶

1239

1240 **Transcriptomics comparison between SeV-stimulated and unstimulated conditions**

1241 Differential expression was performed by comparing (i) each SeV-infected vTR against the SeV-
1242 infected vector control, and (ii) SeV-infected vector controls against uninfected vector controls.

1243 Count matrices were constructed from STARsolo outputs and joined with matched metadata to
1244 ensure consistent gene and sample annotation. DESeq2 (v1.46)¹³² was used with poscounts
1245 normalization to account for sparsity in UMI data, and significance was assessed with
1246 Benjamini–Hochberg correction.

1247 Pathway enrichment was carried out with fgsea (v1.32)(<https://doi.org/10.1101/060012>)
1248 using curated Reactome sets for both comparisons. Genes were ranked by log₂ fold change,
1249 restricted to those present in Reactome sets, and tested with 10,000 permutations. Non-
1250 significant pathways (FDR ≥ 0.05) were set to zero before aggregation into a summary NES
1251 matrix. To highlight construct-specific effects beyond stimulation alone, discordant pathways
1252 were defined as those enriched in opposite directions between stimulated vector controls and
1253 specific stimulated vTRs. These pathways were summarized across vTRs, and clustering of
1254 normalized enrichment scores was used to visualize the relationship between constructs and
1255 pathway-level responses.

1256

1257 **RELI analysis**

1258 To identify which differentially expressed genes (DEGs) resulting from vTR expression were
1259 associated with disease risk loci, we utilized the Regulatory Element Locus Intersection (RELI)
1260 approach as described by Harley et al.¹⁸ RELI statistically tests for enrichment of GWAS risk loci
1261 in user-supplied genomic regions or gene lists, through permutation and comparison to matched
1262 controls. We input the list of up- or down-regulated genes resulting from the expression of each
1263 vTR into RELI and assessed the enrichment of risk-associated loci from published GWAS
1264 datasets proximal to these DEGs (transcription start site +/- 1 kb). Only associations with FDR <
1265 0.05 and at least 5 overlapping loci were considered for further analysis. To determine potential
1266 evidence in the literature for these associations, we annotated reported cases where the virus
1267 encoding for the vTR was associated with the corresponding disease (**Data S7**).

1268 To assess whether hTFs or cofactors (CoFs) may mediate the influence of vTRs on
1269 disease-associated loci, we applied RELI to publicly available hTF/CoF ChIP-seq peak sets
1270 performed in HEK293 (or related) cells. For each hTF/CoF, RELI was used to quantify the
1271 enrichment of GWAS risk loci within ChIP-seq peaks. As in the vTR–DEG analysis, risk loci
1272 were expanded to include variants in linkage disequilibrium with published GWAS variants, and
1273 enrichment was evaluated by comparing the observed overlap to a null distribution generated
1274 through permutation using matched control regions. Significant associations were defined as
1275 hTF/CoF–disease pairs with $p < 0.01$. Next, we integrated these results with the vTR-disease
1276 associations identified in the DEG-based RELI analysis. For a given disease, we identified hTFs
1277 or CoFs that showed significant enrichment at the same GWAS loci for which a vTR was also
1278 significantly associated. To determine whether the vTR could potentially modulate these loci
1279 through recruitment by the hTF/CoF, we required evidence of a PPI between the vTR and the
1280 corresponding hTF/CoF. We annotated all resulting trios where (i) the vTR DEGs were
1281 significantly associated with the disease, (ii) the hTF/CoF ChIP-seq peaks overlapped GWAS
1282 loci for that disease, and (iii) a PPI existed between the vTR and the hTF/CoF (**Data S8**).

1283

1284 **Comparison between hTF and vTR M1H activity**

1285 The transcriptional activities of vTRs were compared to those of hTFs tested by Lambourne et
1286 al. using the low-background M1H system.⁷⁵ The distribution of $\log_2(\text{fold change})$ for all vTRs
1287 tested using the minimal promoter construct described previously was compared to those of
1288 reference hTF isoforms previously tested using the same reporter construct. Distributions were
1289 compared in Prism (Graphpad) using the two-tailed Mann Whitney U-test.

1290

1291 **M1H activity of vTRs with different expression timing**

1292 Annotation of the expression timing of vTRs was performed via literature curation (**Data S9**).
1293 Taking into account the varied expression kinetics of different viruses, we broadly defined

1294 expression timing as follows: Immediate Early (IE) – expressed before replication of the viral
1295 genome. Early (E) – expressed following immediate-early and before replication of the viral
1296 genome. Late (L) – expressed following replication of the viral genome. Early-Late (E/L)
1297 expressed both prior to and following viral genome replication. Latent (Lat) – expressed
1298 primarily or exclusively during viral latency. The transcriptional activities of vTRs expressed at
1299 different timepoints of infection were compared using Prism (Graphpad) via Brown-Forsythe and
1300 Welch multiple ANOVA.

1301

1302 **PROD-ATAC Screen**

1303 PROD-ATAC data analysis (of both the single-cell ATAC libraries and genotyping dial-out
1304 libraries) was performed on the University of Wisconsin-Madison’s Center for High Throughput
1305 Computing cluster as previously described accessed May 2025.¹²⁷ Briefly, single-cell
1306 sequencing datafiles were converted to FASTQ format using cellranger-atac mkfastq (10x
1307 Genomics, version 2.1.0) and aligned to the hg38 reference genome via cellranger-atac count.
1308 Fragment files generated via cellranger-atac count (along with associated cell-assignment file
1309 outputs) were used to build Arrow files in ArchR. ArchR (version 1.0.3) was used for calling vTR
1310 marker peaks and performing downstream analysis using the same filter settings and quality
1311 cutoffs as described in depth previously.¹²⁷ Briefly, all nuclei used for PROD-ATAC data analysis
1312 were first filtered for those with TSS enrichment scores ≥ 7 and $\geq 40,000$ fragments. We then
1313 generated pseudobulk samples representing each vTR genotype and created in silico replicates
1314 to perform statistical tests to identify differentially accessible peaks. The addGroupCoverages
1315 command (minCells=20, maxCells=500, minReplicates=2, maxReplicates=5)
1316 merged cells of a known genotype. The resultant coverage file was queried to identify peaks via
1317 addReproduciblePeakSet. MACS3 was used with default parameters for peak calling. Patterns
1318 of motif enrichment within these differentially accessible peaks were identified by calling
1319 peakAnnoEnrichment with default parameters.

1320 Scripts relevant for downstream PROD-ATAC data processing and figure generation
1321 used in both this and other PROD-ATAC associated publications are deposited in GitHub
1322 (<https://github.com/mfrenkel16/OncofusionPRODATAAC/>).

1323

1324 **Comparing hTF/CoF interactions between viral proteins and vTRs**

1325 Protein interaction partner types for vTRs and non-vTR viral proteins were compared by taking
1326 the union of our Y2H results and interactions compiled by the Human-Virus Interaction
1327 DataBase (HVIDB) (**Data S10**).²² Protein interaction partners of vTRs were categorized into
1328 eight categories: hTF, cofactor, RNA processing, proteostasis, signaling, metabolism, immunity,
1329 or other (**Data S10**). The TF list was obtained from Lambert et al.,⁷⁹ whereas cofactors include
1330 proteins that were not classified as hTF but are annotated in the list of human cofactors from
1331 Animal TF DB.¹³⁷ RNA processing, proteostasis, signaling, metabolism, and immunity were non-
1332 hTF or cofactor proteins that were defined based on gene ontology (GO) terms generated by
1333 UniProt and confirmed via PubMed literature search. Example GO terms for each category are
1334 as follows: RNA processing - regulation of RNA splicing (GO:0043484), mRNA processing
1335 (GO:0006397), mRNA stabilization (GO:0048255), regulation of transcription by RNA
1336 polymerase II (GO:0006357). Proteostasis - protein ubiquitination (GO:0016567), protein folding
1337 (GO:0006457), protein stabilization (GO:0050821), intracellular protein transport (GO:0006886),
1338 . Signaling - signaling (GO:0023052) and related lower terms as described in Lambourne et al.⁷⁵
1339 Metabolism - fatty acid biosynthetic process (GO:0006633), glycolytic process (GO:0006096),
1340 cellular respiration (GO:0045333), ATP biosynthetic process (GO:0006754), TOR signaling
1341 (GO:0031929). Immune - innate immune response (GO:0045087), adaptive immune response
1342 (GO:0002250), inflammatory response (GO:000695), defense response to virus (GO:0051607).
1343 Proportions of interactions with hTF, cofactor, or other (all non-hTF or cofactor proteins) were
1344 then compared between vTRs and non-vTR viral proteins using a permutation test of a χ^2
1345 statistic; two-sided empirical P values were computed.

1346

1347 **Enrichment analysis for different PPI partners across vTR timing**

1348 To assess how different categories of protein interaction partners vary across vTR timing
1349 groups, we first normalized raw interaction counts to per-condition proportions. Proteins were
1350 annotated into functional categories (e.g., hTFs, cofactors, RNA processing, proteostasis,
1351 signaling, metabolism, immunity, and other). For each group, we aggregated proportions across
1352 proteins and compared them to the background average across all conditions. Fold-enrichment
1353 values were calculated, log₂-transformed, and visualized as heatmaps with a fixed scale (± 1.5).
1354 This approach highlights partner categories enriched or depleted in specific vTR timing groups
1355 relative to the overall interaction distribution.

1356

1357 **Comparison between vTR and hTF PPI partners**

1358 Similarity of PPI partners between vTRs and hTFs was assessed by comparing the union of
1359 hTF–human protein interactions supported by at least one piece of evidence in BIOGRID¹³⁸ or
1360 reported in HuRI¹²⁸ with the union of vTR–human protein interactions detected by Y2H (as
1361 described) or reported in HVIDB.²² For each protein partner represented, we calculated the
1362 percentage of hTFs or vTRs with which it interacted. Proteins interacting with more than 5% of
1363 hTFs or vTRs were highlighted. Jaccard indices were calculated to quantify the overlap of PPI
1364 partners: within vTRs, within hTFs, and between vTRs and hTFs.

1365

1366 **Determining structural similarity of homolog vTRs**

1367 Structural similarity of homolog vTRs was determined using NCBI blast to compare amino acid
1368 identities on a pairwise basis. Amino acid sequences were chosen based on the representative
1369 UniProt ID for that given vTR. Amino acid % identity values were rounded to the nearest tenth
1370 place.

1371

1372 References

- 1373 1. Nikoskelainen, J., Panelius, M., and Salmi, A. (1972). E.B. virus and multiple sclerosis. *Br J*
1374 *Med J* 4, 111. <https://doi.org/10.1136/bmj.4.5832.111>.
- 1375 2. Magrath, I. (2012). Epidemiology: clues to the pathogenesis of Burkitt lymphoma. *Br J*
1376 *Haematol* 156, 744–756. <https://doi.org/10.1111/j.1365-2141.2011.09013.x>.
- 1377 3. Marra, F., Gomes, K., Liu, E., Vadlamudi, N.K., Richardson, K., and Cragg, J.J. (2025).
1378 Effects of herpes zoster infection, antivirals and vaccination on risk of developing
1379 dementia: A systematic review and meta-analysis. *Hum Vaccin Immunother* 21, 2546741.
1380 <https://doi.org/10.1080/21645515.2025.2546741>.
- 1381 4. Wolf, J., Kist, L.F., Pereira, S.B., Quessada, M.A., Petek, H., Pille, A., Maccari, J.G.,
1382 Mutlaq, M.P., and Nasi, L.A. (2024). Human papillomavirus infection: Epidemiology,
1383 biology, host interactions, cancer development, prevention, and therapeutics. *Rev Med*
1384 *Virol* 34, e2537. <https://doi.org/10.1002/rmv.2537>.
- 1385 5. Xiao, Q., Liu, Y., Li, T., Wang, C., He, S., Zhai, L., Yang, Z., Zhang, X., Wu, Y., and Liu, Y.
1386 (2025). Viral oncogenesis in cancer: from mechanisms to therapeutics. *Signal Transduct*
1387 *Target Ther* 10, 151. <https://doi.org/10.1038/s41392-025-02197-9>.
- 1388 6. Liu, X., Hong, T., Parameswaran, S., Ernst, K., Marazzi, I., Weirauch, M.T., and Fuxman
1389 Bass, J.I. (2020). Human Virus Transcriptional Regulators. *Cell* 182, 24–37.
1390 <https://doi.org/10.1016/j.cell.2020.06.023>.
- 1391 7. García-Sastre, A. (2017). Ten Strategies of Interferon Evasion by Viruses. *Cell Host*
1392 *Microbe* 22, 176–184. <https://doi.org/10.1016/j.chom.2017.07.012>.
- 1393 8. Katze, M.G., He, Y., and Gale, M. (2002). Viruses and interferon: a fight for supremacy.
1394 *Nat Rev Immunol* 2, 675–687. <https://doi.org/10.1038/nri888>.
- 1395 9. Benedict, C.A., Norris, P.S., and Ware, C.F. (2002). To kill or be killed: viral evasion of
1396 apoptosis. *Nat Immunol* 3, 1013–1018. <https://doi.org/10.1038/ni1102-1013>.
- 1397 10. Mesri, E.A., Feitelson, M.A., and Munger, K. (2014). Human viral oncogenesis: a cancer
1398 hallmarks analysis. *Cell Host Microbe* 15, 266–282.
1399 <https://doi.org/10.1016/j.chom.2014.02.011>.
- 1400 11. Tillo, D., Ray, S., Syed, K.-S., Gaylor, M.R., He, X., Wang, J., Assad, N., Durell, S.R.,
1401 Porollo, A., Weirauch, M.T., et al. (2017). The Epstein-Barr Virus B-ZIP Protein Zta
1402 Recognizes Specific DNA Sequences Containing 5-Methylcytosine and 5-
1403 Hydroxymethylcytosine. *Biochemistry* 56, 6200–6210.
1404 <https://doi.org/10.1021/acs.biochem.7b00741>.
- 1405 12. Ramasubramanyan, S., Osborn, K., Al-Mohammad, R., Naranjo Perez-Fernandez, I.B.,
1406 Zuo, J., Balan, N., Godfrey, A., Patel, H., Peters, G., Rowe, M., et al. (2015). Epstein-Barr
1407 virus transcription factor Zta acts through distal regulatory elements to directly control
1408 cellular gene expression. *Nucleic Acids Res* 43, 3563–3577.
1409 <https://doi.org/10.1093/nar/gkv212>.

- 1410 13. Basbous, J., Arpin, C., Gaudray, G., Piechaczyk, M., Devaux, C., and Mesnard, J.-M.
1411 (2003). The HBZ factor of human T-cell leukemia virus type I dimerizes with transcription
1412 factors JunB and c-Jun and modulates their transcriptional activity. *J Biol Chem* 278,
1413 43620–43627. <https://doi.org/10.1074/jbc.M307275200>.
- 1414 14. Ferrari, R., Pellegrini, M., Horwitz, G.A., Xie, W., Berk, A.J., and Kurdistani, S.K. (2008).
1415 Epigenetic reprogramming by adenovirus e1a. *Science* 321, 1086–1088.
1416 <https://doi.org/10.1126/science.1155546>.
- 1417 15. Guerrieri, F., Belloni, L., D’Andrea, D., Pediconi, N., Le Pera, L., Testoni, B., Scisciani, C.,
1418 Floriot, O., Zoulim, F., Tramontano, A., et al. (2017). Genome-wide identification of direct
1419 HBx genomic targets. *BMC Genomics* 18, 184. <https://doi.org/10.1186/s12864-017-3561-5>.
- 1420 16. Patrick, D.R., Oliff, A., and Heimbrook, D.C. (1994). Identification of a novel retinoblastoma
1421 gene product binding site on human papillomavirus type 16 E7 protein. *J Biol Chem* 269,
1422 6842–6850.
- 1423 17. Miyazawa, M., Noguchi, K., Kujirai, M., Katayama, K., Yamagoe, S., and Sugimoto, Y.
1424 (2018). IL-10 promoter transactivation by the viral K-RTA protein involves the host-cell
1425 transcription factors, specificity proteins 1 and 3. *J Biol Chem* 293, 662–676.
1426 <https://doi.org/10.1074/jbc.M117.802900>.
- 1427 18. Harley, J.B., Chen, X., Pujato, M., Miller, D., Maddox, A., Forney, C., Magnusen, A.F.,
1428 Lynch, A., Chetal, K., Yukawa, M., et al. (2018). Transcription factors operate across
1429 disease loci, with EBNA2 implicated in autoimmunity. *Nat Genet* 50, 699–707.
1430 <https://doi.org/10.1038/s41588-018-0102-3>.
- 1431 19. Hong, T., Parameswaran, S., Donmez, O.A., Miller, D., Forney, C., Lape, M., Saint Just
1432 Ribeiro, M., Liang, J., Edsall, L.E., Magnusen, A.F., et al. (2021). Epstein-Barr virus
1433 nuclear antigen 2 extensively rewires the human chromatin landscape at autoimmune risk
1434 loci. *Genome Res* 31, 2185–2198. <https://doi.org/10.1101/gr.264705.120>.
- 1435 20. Dexheimer, P.J., Hass, M.R., Edsall, L.E., Diouf, A.A., Jones, S.H., Donmez, O., Yin, C.,
1436 Dunn, K.A., Forney, C., Hesse, H.K., et al. (2025). Systematic investigation reveals
1437 extensive Epstein-Barr virus transcriptional regulation of the human genome. *bioRxiv*,
1438 2025.07.18.665561. <https://doi.org/10.1101/2025.07.18.665561>.
- 1439 21. Massimino, L., Palmieri, O., Facoetti, A., Fuggetta, D., Spanò, S., Lamparelli, L.A.,
1440 D’Alessio, S., Cagliani, S., Furfaro, F., D’Amico, F., et al. (2023). Gut virome-colonising
1441 Orthohepadnavirus genus is associated with ulcerative colitis pathogenesis and induces
1442 intestinal inflammation in vivo. *Gut* 72, 1838–1847. <https://doi.org/10.1136/gutjnl-2022-328375>.
- 1444 22. Yang, X., Lian, X., Fu, C., Wuchty, S., Yang, S., and Zhang, Z. (2021). HVIDB: a
1445 comprehensive database for human-virus protein-protein interactions. *Brief Bioinform* 22,
1446 832–844. <https://doi.org/10.1093/bib/bbaa425>.
- 1447 23. Ludwig, C.H., Thurm, A.R., Morgens, D.W., Yang, K.J., Tycko, J., Bassik, M.C.,
1448 Glaunsinger, B.A., and Bintu, L. (2023). High-throughput discovery and characterization of
1449 viral transcriptional effectors in human cells. *Cell Syst* 14, 482-500.e8.
1450 <https://doi.org/10.1016/j.cels.2023.05.008>.

- 1451 24. Alpern, D., Gardeux, V., Russeil, J., Mangeat, B., Meireles-Filho, A.C.A., Breyse, R.,
1452 Hacker, D., and Deplancke, B. (2019). BRB-seq: ultra-affordable high-throughput
1453 transcriptomics enabled by bulk RNA barcoding and sequencing. *Genome Biol* 20, 71.
1454 <https://doi.org/10.1186/s13059-019-1671-x>.
- 1455 25. Santoso, C.S., Li, Z., Lal, S., Yuan, S., Gan, K.A., Agosto, L.M., Liu, X., Pro, S.C., Sewell,
1456 J.A., Henderson, A., et al. (2020). Comprehensive mapping of the human cytokine gene
1457 regulatory network. *Nucleic Acids Res* 48, 12055–12073.
1458 <https://doi.org/10.1093/nar/gkaa1055>.
- 1459 26. Berenson, A., Lane, R., Soto-Ugaldi, L.F., Patel, M., Ciausiu, C., Li, Z., Chen, Y., Shah, S.,
1460 Santoso, C., Liu, X., et al. (2023). Paired yeast one-hybrid assays to detect DNA-binding
1461 cooperativity and antagonism across transcription factors. *Nat Commun* 14, 6570.
1462 <https://doi.org/10.1038/s41467-023-42445-6>.
- 1463 27. Shin, Y.C., Nakamura, H., Liang, X., Feng, P., Chang, H., Kowalik, T.F., and Jung, J.U.
1464 (2006). Inhibition of the ATM/p53 signal transduction pathway by Kaposi's sarcoma-
1465 associated herpesvirus interferon regulatory factor 1. *J Virol* 80, 2257–2266.
1466 <https://doi.org/10.1128/JVI.80.5.2257-2266.2006>.
- 1467 28. Lee, H.-R., Kim, M.H., Lee, J.-S., Liang, C., and Jung, J.U. (2009). Viral interferon
1468 regulatory factors. *J Interferon Cytokine Res* 29, 621–627.
1469 <https://doi.org/10.1089/jir.2009.0067>.
- 1470 29. zur Hausen, H. (2002). Papillomaviruses and cancer: from basic studies to clinical
1471 application. *Nat Rev Cancer* 2, 342–350. <https://doi.org/10.1038/nrc798>.
- 1472 30. Zhang, Y., Qiu, K., Ren, J., Zhao, Y., and Cheng, P. (2025). Roles of human
1473 papillomavirus in cancers: oncogenic mechanisms and clinical use. *Signal Transduct*
1474 *Target Ther* 10, 44. <https://doi.org/10.1038/s41392-024-02083-w>.
- 1475 31. Fuxman Bass, J.I., Diallo, A., Nelson, J., Soto, J.M., Myers, C.L., and Walhout, A.J.M.
1476 (2013). Using networks to measure similarity between genes: association index selection.
1477 *Nat Methods* 10, 1169–1176. <https://doi.org/10.1038/nmeth.2728>.
- 1478 32. Green, R.A., Kao, H.-L., Audhya, A., Arur, S., Mayers, J.R., Fridolfsson, H.N., Schulman,
1479 M., Schloissnig, S., Niessen, S., Laband, K., et al. (2011). A high-resolution *C. elegans*
1480 essential gene network based on phenotypic profiling of a complex tissue. *Cell* 145, 470–
1481 482. <https://doi.org/10.1016/j.cell.2011.03.037>.
- 1482 33. Azran, I., Schavinsky-Khrapunsky, Y., and Aboud, M. (2004). Role of Tax protein in human
1483 T-cell leukemia virus type-I leukemogenicity. *Retrovirology* 1, 20.
1484 <https://doi.org/10.1186/1742-4690-1-20>.
- 1485 34. Müller, S., and Dejean, A. (1999). Viral immediate-early proteins abrogate the modification
1486 by SUMO-1 of PML and Sp100 proteins, correlating with nuclear body disruption. *J Virol*
1487 73, 5137–5143. <https://doi.org/10.1128/JVI.73.6.5137-5143.1999>.
- 1488 35. Harwardt, T., Lukas, S., Zenger, M., Reitberger, T., Danzer, D., Übner, T., Munday, D.C.,
1489 Nevels, M., and Paulus, C. (2016). Human Cytomegalovirus Immediate-Early 1 Protein
1490 Rewires Upstream STAT3 to Downstream STAT1 Signaling Switching an IL6-Type to an

- 1491 IFN γ -Like Response. *PLoS Pathog* 12, e1005748.
1492 <https://doi.org/10.1371/journal.ppat.1005748>.
- 1493 36. Kirchhoff, S., Sebens, T., Baumann, S., Krueger, A., Zawatzky, R., Li-Weber, M., Meinel, E.,
1494 Neipel, F., Fleckenstein, B., and Krammer, P.H. (2002). Viral IFN-regulatory factors inhibit
1495 activation-induced cell death via two positive regulatory IFN-regulatory factor 1-dependent
1496 domains in the CD95 ligand promoter. *J Immunol* 168, 1226–1234.
1497 <https://doi.org/10.4049/jimmunol.168.3.1226>.
- 1498 37. Lin, R., Genin, P., Mamane, Y., Sgarbanti, M., Battistini, A., Harrington, W.J., Barber, G.N.,
1499 and Hiscott, J. (2001). HHV-8 encoded vIRF-1 represses the interferon antiviral response
1500 by blocking IRF-3 recruitment of the CBP/p300 coactivators. *Oncogene* 20, 800–811.
1501 <https://doi.org/10.1038/sj.onc.1204163>.
- 1502 38. Ross, T.M., Narayan, M., Fang, Z.Y., Minella, A.C., and Green, P.L. (2000). Human T-cell
1503 leukemia virus type 2 tax mutants that selectively abrogate NF κ B or CREB/ATF
1504 activation fail to transform primary human T cells. *J Virol* 74, 2655–2662.
1505 <https://doi.org/10.1128/jvi.74.6.2655-2662.2000>.
- 1506 39. Bertzbach, L.D., Seddar, L., von Stromberg, K., Ip, W.-H., Dobner, T., and Hidalgo, P.
1507 (2024). The adenovirus DNA-binding protein DBP. *J Virol* 98, e0188523.
1508 <https://doi.org/10.1128/jvi.01885-23>.
- 1509 40. Khetan, S., Carroll, B.S., and Bulyk, M.L. (2025). Multiple overlapping binding sites
1510 determine transcription factor occupancy. *Nature* 646, 1001–1011.
1511 <https://doi.org/10.1038/s41586-025-09472-3>.
- 1512 41. Lara-Pezzi, E., Majano, P.L., Gómez-Gonzalo, M., García-Monzón, C., Moreno-Otero, R.,
1513 Levrero, M., and López-Cabrera, M. (1998). The hepatitis B virus X protein up-regulates
1514 tumor necrosis factor alpha gene expression in hepatocytes. *Hepatology* 28, 1013–1021.
1515 <https://doi.org/10.1002/hep.510280416>.
- 1516 42. Terradillos, O., Billet, O., Renard, C.A., Levy, R., Molina, T., Briand, P., and Buendia, M.A.
1517 (1997). The hepatitis B virus X gene potentiates c-myc-induced liver oncogenesis in
1518 transgenic mice. *Oncogene* 14, 395–404. <https://doi.org/10.1038/sj.onc.1200850>.
- 1519 43. Plakogiannis, F.M., Mahzouf, S.Z., and Babar, A. (1989). Determination of the optimum
1520 solvent system for extraction of minoxidil from a tablet dosage form. *Pharm Acta Helv* 64,
1521 348–350.
- 1522 44. Chen, Z., Tang, J., Cai, X., Huang, Y., Gao, Q., Liang, L., Tian, L., Yang, Y., Zheng, Y.,
1523 Hu, Y., et al. (2016). HBx mutations promote hepatoma cell migration through the Wnt/ β -
1524 catenin signaling pathway. *Cancer Sci* 107, 1380–1389. <https://doi.org/10.1111/cas.13014>.
- 1525 45. Zheng, B.-Y., Gao, W.-Y., Huang, X.-Y., Lin, L.-Y., Fang, X.-F., Chen, Z.-X., and Wang, X.-
1526 Z. (2018). HBx promotes the proliferative ability of HL \square 7702 cells via the
1527 COX \square 2/Wnt/ β \square catenin pathway. *Mol Med Rep* 17, 8432–8438.
1528 <https://doi.org/10.3892/mmr.2018.8906>.

- 1529 46. Duyao, M.P., Kessler, D.J., Spicer, D.B., and Sonenshein, G.E. (1992). Transactivation of
1530 the c-myc gene by HTLV-1 tax is mediated by NFκB. *Curr Top Microbiol Immunol* 182,
1531 421–424. https://doi.org/10.1007/978-3-642-77633-5_53.
- 1532 47. Poirson, J., Suarez, I.P., Straub, M.-L., Cousido-Siah, A., Peixoto, P., Hervouet, E., Foster,
1533 A., Mitschler, A., Mukobo, N., Chebaro, Y., et al. (2022). High-Risk Mucosal Human
1534 Papillomavirus 16 (HPV16) E6 Protein and Cutaneous HPV5 and HPV8 E6 Proteins
1535 Employ Distinct Strategies To Interfere with Interferon Regulatory Factor 3-Mediated Beta
1536 Interferon Expression. *J Virol* 96, e0187521. <https://doi.org/10.1128/jvi.01875-21>.
- 1537 48. Castro-Muñoz, L.J., Rocha-Zavaleta, L., Lizano, M., Ramírez-Alcántara, K.M., Madrid-
1538 Marina, V., and Manzo-Merino, J. (2022). Alteration of the IFN-Pathway by Human
1539 Papillomavirus Proteins: Antiviral Immune Response Evasion Mechanism. *Biomedicines*
1540 10, 2965. <https://doi.org/10.3390/biomedicines10112965>.
- 1541 49. Um, S.-J., Rhyu, J.-W., Kim, E.-J., Jeon, K.-C., Hwang, E.-S., and Park, J.-S. (2002).
1542 Abrogation of IRF-1 response by high-risk HPV E7 protein in vivo. *Cancer Lett* 179, 205–
1543 212. [https://doi.org/10.1016/s0304-3835\(01\)00871-0](https://doi.org/10.1016/s0304-3835(01)00871-0).
- 1544 50. Ronco, L.V., Karpova, A.Y., Vidal, M., and Howley, P.M. (1998). Human papillomavirus 16
1545 E6 oncoprotein binds to interferon regulatory factor-3 and inhibits its transcriptional activity.
1546 *Genes Dev* 12, 2061–2072. <https://doi.org/10.1101/gad.12.13.2061>.
- 1547 51. Li, W.-F., Alfason, L., Huang, C., Tang, Y., Qiu, L., Miyagishi, M., Wu, S.-R., and Kasim, V.
1548 (2023). p52-ZER6: a determinant of tumor cell sensitivity to MDM2-p53 binding inhibitors.
1549 *Acta Pharmacol Sin* 44, 647–660. <https://doi.org/10.1038/s41401-022-00973-9>.
- 1550 52. Huang, C., Wu, S., Li, W., Herkilini, A., Miyagishi, M., Zhao, H., and Kasim, V. (2019).
1551 Zinc-finger protein p52-ZER6 accelerates colorectal cancer cell proliferation and tumour
1552 progression through promoting p53 ubiquitination. *EBioMedicine* 48, 248–263.
1553 <https://doi.org/10.1016/j.ebiom.2019.08.070>.
- 1554 53. Qiu, L., Li, W., Zhang, L., Zhang, X., Zhao, H., Miyagishi, M., Wu, S., and Kasim, V.
1555 (2025). p52-ZER6/DAZAP1 axis promotes ferroptosis resistance and colorectal cancer
1556 progression via regulating SLC7A11 mRNA stabilization. *Acta Pharm Sin B* 15, 2039–
1557 2058. <https://doi.org/10.1016/j.apsb.2025.02.013>.
- 1558 54. Tang, Y., Li, W., Qiu, L., Zhang, X., Zhang, L., Miyagishi, M., Zhao, H., Wu, S., and Kasim,
1559 V. (2023). The p52-ZER6/G6PD axis alters aerobic glycolysis and promotes tumor
1560 progression by activating the pentose phosphate pathway. *Oncogenesis* 12, 17.
1561 <https://doi.org/10.1038/s41389-023-00464-4>.
- 1562 55. Li, W., Huang, C., Qiu, L., Tang, Y., Zhang, X., Zhang, L., Zhao, H., Miyagishi, M., Kasim,
1563 V., and Wu, S. (2024). p52-ZER6/IGF1R axis maintains cancer stem cell population to
1564 promote cancer progression by enhancing pro-survival mitophagy. *Oncogene* 43, 2115–
1565 2131. <https://doi.org/10.1038/s41388-024-03058-5>.
- 1566 56. Chellappan, S., Kraus, V.B., Kroger, B., Munger, K., Howley, P.M., Phelps, W.C., and
1567 Nevins, J.R. (1992). Adenovirus E1A, simian virus 40 tumor antigen, and human
1568 papillomavirus E7 protein share the capacity to disrupt the interaction between

- 1569 transcription factor E2F and the retinoblastoma gene product. *Proc Natl Acad Sci U S A*
1570 89, 4549–4553. <https://doi.org/10.1073/pnas.89.10.4549>.
- 1571 57. Wu, E.W., Clemens, K.E., Heck, D.V., and Münger, K. (1993). The human papillomavirus
1572 E7 oncoprotein and the cellular transcription factor E2F bind to separate sites on the
1573 retinoblastoma tumor suppressor protein. *J Virol* 67, 2402–2407.
1574 <https://doi.org/10.1128/JVI.67.4.2402-2407.1993>.
- 1575 58. Caberg, J.-H.D., Hubert, P.M., Begon, D.Y., Herfs, M.F., Roncarati, P.J., Boniver, J.J., and
1576 Delvenne, P.O. (2008). Silencing of E7 oncogene restores functional E-cadherin
1577 expression in human papillomavirus 16-transformed keratinocytes. *Carcinogenesis* 29,
1578 1441–1447. <https://doi.org/10.1093/carcin/bgn145>.
- 1579 59. Hahn, S., and Hermeking, H. (2014). ZNF281/ZBP-99: a new player in epithelial-
1580 mesenchymal transition, stemness, and cancer. *J Mol Med (Berl)* 92, 571–581.
1581 <https://doi.org/10.1007/s00109-014-1160-3>.
- 1582 60. Zhao, Q., Zhang, C., Zhang, X., Wang, S., Guo, T., Yin, Y., Zhang, H., Li, Z., Si, Y., Lu, Y.,
1583 et al. (2023). ZNF281 inhibits mitochondrial biogenesis to facilitate metastasis of
1584 hepatocellular carcinoma. *Cell Death Discov* 9, 396. <https://doi.org/10.1038/s41420-023-01691-9>.
- 1586 61. Lu, C., Ge, T., Shao, Y., Cui, W., Li, Z., Xu, W., and Bao, X. (2023). ZNF281 drives
1587 hepatocyte senescence in alcoholic liver disease by reducing HK2-
1588 stabilized PINK1/Parkin-mediated mitophagy. *Cell Prolif* 56, e13378.
1589 <https://doi.org/10.1111/cpr.13378>.
- 1590 62. Pierdomenico, M., Palone, F., Cesi, V., Vitali, R., Mancuso, A.B., Cucchiara, S., Oliva, S.,
1591 Aloï, M., and Stronati, L. (2018). Transcription Factor ZNF281: A Novel Player in Intestinal
1592 Inflammation and Fibrosis. *Front Immunol* 9, 2907.
1593 <https://doi.org/10.3389/fimmu.2018.02907>.
- 1594 63. Taylor, R.T., and Bresnahan, W.A. (2005). Human cytomegalovirus immediate-early 2
1595 gene expression blocks virus-induced beta interferon production. *J Virol* 79, 3873–3877.
1596 <https://doi.org/10.1128/JVI.79.6.3873-3877.2005>.
- 1597 64. Zhang, X., Wang, Q., Han, S., Song, G., Wang, B., and Wang, Y. (2025). Human
1598 cytomegalovirus-IE2 suppresses antigen presentation of macrophage through the
1599 IL10/STAT3 signalling pathway in transgenic mouse. *PLoS One* 20, e0322334.
1600 <https://doi.org/10.1371/journal.pone.0322334>.
- 1601 65. Heilingloh, C.S., Grosche, L., Kummer, M., Mühl-Zürbes, P., Kamm, L., Scherer, M.,
1602 Latzko, M., Stamminger, T., and Steinkasserer, A. (2017). The Major Immediate-Early
1603 Protein IE2 of Human Cytomegalovirus Is Sufficient to Induce Proteasomal Degradation of
1604 CD83 on Mature Dendritic Cells. *Front Microbiol* 8, 119.
1605 <https://doi.org/10.3389/fmicb.2017.00119>.
- 1606 66. Kim, J.-E., Kim, Y.-E., Stinski, M.F., Ahn, J.-H., and Song, Y.-J. (2017). Human
1607 Cytomegalovirus IE2 86 kDa Protein Induces STING Degradation and Inhibits cGAMP-
1608 Mediated IFN- β Induction. *Front Microbiol* 8, 1854.
1609 <https://doi.org/10.3389/fmicb.2017.01854>.

- 1610 67. Horwitz, G.A., Zhang, K., McBrian, M.A., Grunstein, M., Kurdistani, S.K., and Berk, A.J.
1611 (2008). Adenovirus small e1a alters global patterns of histone modification. *Science* *321*,
1612 1084–1085. <https://doi.org/10.1126/science.1155544>.
- 1613 68. Schaeffner, M., Mrozek-Gorska, P., Buschle, A., Woellmer, A., Tagawa, T., Cernilogar,
1614 F.M., Schotta, G., Krietenstein, N., Lieleg, C., Korber, P., et al. (2019). BZLF1 interacts
1615 with chromatin remodelers promoting escape from latent infections with EBV. *Life Sci*
1616 *Alliance* *2*, e201800108. <https://doi.org/10.26508/lsa.201800108>.
- 1617 69. Pumfery, A., Deng, L., Maddukuri, A., de la Fuente, C., Li, H., Wade, J.D., Lambert, P.,
1618 Kumar, A., and Kashanchi, F. (2003). Chromatin remodeling and modification during HIV-1
1619 Tat-activated transcription. *Curr HIV Res* *1*, 343–362.
1620 <https://doi.org/10.2174/1570162033485186>.
- 1621 70. Nevels, M., Rubenwolf, S., Spruss, T., Wolf, H., and Dobner, T. (2000). Two distinct
1622 activities contribute to the oncogenic potential of the adenovirus type 5 E4orf6 protein. *J*
1623 *Virol* *74*, 5168–5181. <https://doi.org/10.1128/jvi.74.11.5168-5181.2000>.
- 1624 71. Yamano, S., Tokino, T., Yasuda, M., Kaneuchi, M., Takahashi, M., Niitsu, Y., Fujinaga, K.,
1625 and Yamashita, T. (1999). Induction of transformation and p53-dependent apoptosis by
1626 adenovirus type 5 E4orf6/7 cDNA. *J Virol* *73*, 10095–10103.
1627 <https://doi.org/10.1128/JVI.73.12.10095-10103.1999>.
- 1628 72. Boivin, D., Morrison, M.R., Marcellus, R.C., Querido, E., and Branton, P.E. (1999).
1629 Analysis of synthesis, stability, phosphorylation, and interacting polypeptides of the 34-
1630 kilodalton product of open reading frame 6 of the early region 4 protein of human
1631 adenovirus type 5. *J Virol* *73*, 1245–1253. <https://doi.org/10.1128/JVI.73.2.1245-1253.1999>.
- 1633 73. Soto, L.F., Li, Z., Santoso, C.S., Berenson, A., Ho, I., Shen, V.X., Yuan, S., and Fuxman
1634 Bass, J.I. (2022). Compendium of human transcription factor effector domains. *Mol Cell* *82*,
1635 514–526. <https://doi.org/10.1016/j.molcel.2021.11.007>.
- 1636 74. Mukund, A.X., Tycko, J., Allen, S.J., Robinson, S.A., Andrews, C., Sinha, J., Ludwig, C.H.,
1637 Spees, K., Bassik, M.C., and Bintu, L. (2023). High-throughput functional characterization
1638 of combinations of transcriptional activators and repressors. *Cell Syst* *14*, 746-763.e5.
1639 <https://doi.org/10.1016/j.cels.2023.07.001>.
- 1640 75. Lambourne, L., Mattioli, K., Santoso, C., Sheynkman, G., Inukai, S., Kaundal, B.,
1641 Berenson, A., Spirohn-Fitzgerald, K., Bhattacharjee, A., Rothman, E., et al. (2025).
1642 Widespread variation in molecular interactions and regulatory properties among
1643 transcription factor isoforms. *Mol Cell* *85*, 1445-1466.e13.
1644 <https://doi.org/10.1016/j.molcel.2025.03.004>.
- 1645 76. Lambourne, L., Mattioli, K., Santoso, C., Sheynkman, G., Inukai, S., Kaundal, B.,
1646 Berenson, A., Spirohn-Fitzgerald, K., Bhattacharjee, A., Rothman, E., et al. (2024).
1647 Widespread variation in molecular interactions and regulatory properties among
1648 transcription factor isoforms. *bioRxiv*, 2024.03.12.584681.
1649 <https://doi.org/10.1101/2024.03.12.584681>.

- 1650 77. Fan, D., Wang, M., Cheng, A., Jia, R., Yang, Q., Wu, Y., Zhu, D., Zhao, X., Chen, S., Liu,
1651 M., et al. (2020). The Role of VP16 in the Life Cycle of Alphaherpesviruses. *Front Microbiol*
1652 *11*, 1910. <https://doi.org/10.3389/fmicb.2020.01910>.
- 1653 78. Chen, H., and Pugh, B.F. (2021). What do Transcription Factors Interact With? *J Mol Biol*
1654 *433*, 166883. <https://doi.org/10.1016/j.jmb.2021.166883>.
- 1655 79. Lambert, S.A., Jolma, A., Campitelli, L.F., Das, P.K., Yin, Y., Albu, M., Chen, X., Taipale,
1656 J., Hughes, T.R., and Weirauch, M.T. (2018). The Human Transcription Factors. *Cell* *172*,
1657 650–665. <https://doi.org/10.1016/j.cell.2018.01.029>.
- 1658 80. Yan, C., Dodd, T., He, Y., Tainer, J.A., Tsutakawa, S.E., and Ivanov, I. (2019).
1659 Transcription preinitiation complex structure and dynamics provide insight into genetic
1660 diseases. *Nat Struct Mol Biol* *26*, 397–406. <https://doi.org/10.1038/s41594-019-0220-3>.
- 1661 81. Inge, M.M., Miller, R., Hook, H., Bray, D., Keenan, J.L., Zhao, R., Gilmore, T.D., and
1662 Siggers, T. (2024). Rapid profiling of transcription factor-cofactor interaction networks
1663 reveals principles of epigenetic regulation. *Nucleic Acids Res* *52*, 10276–10296.
1664 <https://doi.org/10.1093/nar/gkae706>.
- 1665 82. Panne, D., Maniatis, T., and Harrison, S.C. (2007). An atomic model of the interferon-beta
1666 enhanceosome. *Cell* *129*, 1111–1123. <https://doi.org/10.1016/j.cell.2007.05.019>.
- 1667 83. Guirimand, T., Delmotte, S., and Navratil, V. (2015). VirHostNet 2.0: surfing on the web of
1668 virus/host molecular interactions data. *Nucleic Acids Res* *43*, D583-587.
1669 <https://doi.org/10.1093/nar/gku1121>.
- 1670 84. Calderone, A., Licata, L., and Cesareni, G. (2015). VirusMentha: a new resource for virus-
1671 host protein interactions. *Nucleic Acids Res* *43*, D588-592.
1672 <https://doi.org/10.1093/nar/gku830>.
- 1673 85. Chen, G., and Courey, A.J. (2000). Groucho/TLE family proteins and transcriptional
1674 repression. *Gene* *249*, 1–16. [https://doi.org/10.1016/s0378-1119\(00\)00161-x](https://doi.org/10.1016/s0378-1119(00)00161-x).
- 1675 86. Yu, G., Chen, Y., Hu, Y., Zhou, Y., Ding, X., and Zhou, X. (2022). Roles of transducin-like
1676 enhancer of split (TLE) family proteins in tumorigenesis and immune regulation. *Front Cell*
1677 *Dev Biol* *10*, 1010639. <https://doi.org/10.3389/fcell.2022.1010639>.
- 1678 87. Beagle, B., and Johnson, G.V.W. (2010). AES/GRG5: more than just a dominant-negative
1679 TLE/GRG family member. *Dev Dyn* *239*, 2795–2805. <https://doi.org/10.1002/dvdy.22439>.
- 1680 88. Candia, A.F., Hu, J., Crosby, J., Lalley, P.A., Noden, D., Nadeau, J.H., and Wright, C.V.
1681 (1992). Mox-1 and Mox-2 define a novel homeobox gene subfamily and are differentially
1682 expressed during early mesodermal patterning in mouse embryos. *Development* *116*,
1683 1123–1136. <https://doi.org/10.1242/dev.116.4.1123>.
- 1684 89. Candia, A.F., and Wright, C.V. (1996). Differential localization of Mox-1 and Mox-2 proteins
1685 indicates distinct roles during development. *Int J Dev Biol* *40*, 1179–1184.

- 1686 90. He, L., Yuan, L., Yu, W., Sun, Y., Jiang, D., Wang, X., Feng, X., Wang, Z., Xu, J., Yang,
1687 R., et al. (2020). A Regulation Loop between YAP and NR4A1 Balances Cell Proliferation
1688 and Apoptosis. *Cell Rep* 33, 108284. <https://doi.org/10.1016/j.celrep.2020.108284>.
- 1689 91. Fassett, M.S., Jiang, W., D'Alise, A.M., Mathis, D., and Benoist, C. (2012). Nuclear
1690 receptor Nr4a1 modulates both regulatory T-cell (Treg) differentiation and clonal deletion.
1691 *Proc Natl Acad Sci U S A* 109, 3891–3896. <https://doi.org/10.1073/pnas.1200090109>.
- 1692 92. Gao, Y., Zou, Y., Sokolowski, D., Xing, X., Tower, R.J., Lai, Z., Shi, J., Zhu, L., Zheng, Q.,
1693 James, A.W., et al. (2024). Nr4a1 enhances Wnt4 transcription to promote mesenchymal
1694 stem cell osteogenesis and alleviates inflammation-inhibited bone regeneration. *Mol Ther*
1695 32, 1479–1496. <https://doi.org/10.1016/j.ymthe.2024.02.034>.
- 1696 93. Goodrich, D.W., Wang, N.P., Qian, Y.W., Lee, E.Y., and Lee, W.H. (1991). The
1697 retinoblastoma gene product regulates progression through the G1 phase of the cell cycle.
1698 *Cell* 67, 293–302. [https://doi.org/10.1016/0092-8674\(91\)90181-w](https://doi.org/10.1016/0092-8674(91)90181-w).
- 1699 94. Pagano, M., Pepperkok, R., Verde, F., Ansorge, W., and Draetta, G. (1992). Cyclin A is
1700 required at two points in the human cell cycle. *EMBO J* 11, 961–971.
1701 <https://doi.org/10.1002/j.1460-2075.1992.tb05135.x>.
- 1702 95. Rogers, R.P., Woisetschlaeger, M., and Speck, S.H. (1990). Alternative splicing dictates
1703 translational start in Epstein-Barr virus transcripts. *EMBO J* 9, 2273–2277.
1704 <https://doi.org/10.1002/j.1460-2075.1990.tb07398.x>.
- 1705 96. Cohrs, R.J., and Gilden, D.H. (2001). Human herpesvirus latency. *Brain Pathol* 11, 465–
1706 474. <https://doi.org/10.1111/j.1750-3639.2001.tb00415.x>.
- 1707 97. Reichelt, M., Brady, J., and Arvin, A.M. (2009). The replication cycle of varicella-zoster
1708 virus: analysis of the kinetics of viral protein expression, genome synthesis, and virion
1709 assembly at the single-cell level. *J Virol* 83, 3904–3918. <https://doi.org/10.1128/JVI.02137-08>.
1710
- 1711 98. Chen, J.J., Zhu, Z., Gershon, A.A., and Gershon, M.D. (2004). Mannose 6-phosphate
1712 receptor dependence of varicella zoster virus infection in vitro and in the epidermis during
1713 varicella and zoster. *Cell* 119, 915–926. <https://doi.org/10.1016/j.cell.2004.11.007>.
- 1714 99. Rogers, J.M., Guo, B., Egan, E.D., Aster, J.C., Adelman, K., and Blacklow, S.C. (2020).
1715 MAML1-Dependent Notch-Responsive Genes Exhibit Differing Cofactor Requirements for
1716 Transcriptional Activation. *Mol Cell Biol* 40, e00014-20.
1717 <https://doi.org/10.1128/MCB.00014-20>.
- 1718 100. Chand, V., Nandi, D., Mangla, A.G., Sharma, P., and Nag, A. (2016). Tale of a multifaceted
1719 co-activator, hADA3: from embryogenesis to cancer and beyond. *Open Biol* 6, 160153.
1720 <https://doi.org/10.1098/rsob.160153>.
- 1721 101. Münz, C., Lünemann, J.D., Getts, M.T., and Miller, S.D. (2009). Antiviral immune
1722 responses: triggers of or triggered by autoimmunity? *Nat Rev Immunol* 9, 246–258.
1723 <https://doi.org/10.1038/nri2527>.

- 1724 102. Fujinami, R.S., von Herrath, M.G., Christen, U., and Whitton, J.L. (2006). Molecular
1725 mimicry, bystander activation, or viral persistence: infections and autoimmune disease.
1726 *Clin Microbiol Rev* 19, 80–94. <https://doi.org/10.1128/CMR.19.1.80-94.2006>.
- 1727 103. Keane, J.T., Afrasiabi, A., Schibeci, S.D., Swaminathan, S., Parnell, G.P., and Booth, D.R.
1728 (2021). The interaction of Epstein-Barr virus encoded transcription factor EBNA2 with
1729 multiple sclerosis risk loci is dependent on the risk genotype. *EBioMedicine* 71, 103572.
1730 <https://doi.org/10.1016/j.ebiom.2021.103572>.
- 1731 104. Viel, K.C.M.F., Parameswaran, S., Donmez, O.A., Forney, C.R., Hass, M.R., Yin, C.,
1732 Jones, S.H., Prosser, H.K., Diouf, A.A., Gittens, O.E., et al. (2024). Shared and distinct
1733 interactions of type 1 and type 2 Epstein-Barr Nuclear Antigen 2 with the human genome.
1734 *BMC Genomics* 25, 273. <https://doi.org/10.1186/s12864-024-10183-8>.
- 1735 105. Ricigliano, V.A.G., Handel, A.E., Sandve, G.K., Annibali, V., Ristori, G., Mechelli, R.,
1736 Cader, M.Z., and Salvetti, M. (2015). EBNA2 binds to genomic intervals associated with
1737 multiple sclerosis and overlaps with vitamin D receptor occupancy. *PLoS One* 10,
1738 e0119605. <https://doi.org/10.1371/journal.pone.0119605>.
- 1739 106. Nikitskaya, E., Lebedeva, A., Ivanova, O., Maryukhnich, E., Shpektor, A., Grivel, J.-C.,
1740 Margolis, L., and Vasilieva, E. (2016). Cytomegalovirus-Productive Infection Is Associated
1741 With Acute Coronary Syndrome. *J Am Heart Assoc* 5, e003759.
1742 <https://doi.org/10.1161/JAHA.116.003759>.
- 1743 107. Wang, H., Peng, G., Bai, J., He, B., Huang, K., Hu, X., and Liu, D. (2017). Cytomegalovirus
1744 Infection and Relative Risk of Cardiovascular Disease (Ischemic Heart Disease, Stroke,
1745 and Cardiovascular Death): A Meta-Analysis of Prospective Studies Up to 2016. *J Am*
1746 *Heart Assoc* 6, e005025. <https://doi.org/10.1161/JAHA.116.005025>.
- 1747 108. Tanaka, K., Zou, J.P., Takeda, K., Ferrans, V.J., Sandford, G.R., Johnson, T.M., Finkel, T.,
1748 and Epstein, S.E. (1999). Effects of human cytomegalovirus immediate-early proteins on
1749 p53-mediated apoptosis in coronary artery smooth muscle cells. *Circulation* 99, 1656–
1750 1659. <https://doi.org/10.1161/01.cir.99.13.1656>.
- 1751 109. Ma, G., Yu, Z., Nan, F., Zhang, X., Jiang, S., Wang, Y., and Wang, B. (2023). HCMV-IE2
1752 promotes atherosclerosis by inhibiting vascular smooth muscle cells' pyroptosis. *Front*
1753 *Microbiol* 14, 1177391. <https://doi.org/10.3389/fmicb.2023.1177391>.
- 1754 110. Wu, C.-C., Jiang, X., Wang, X.-Z., Liu, X.-J., Li, X.-J., Yang, B., Ye, H.-Q., Harwardt, T.,
1755 Jiang, M., Xia, H.-M., et al. (2018). Human Cytomegalovirus Immediate Early 1 Protein
1756 Causes Loss of SOX2 from Neural Progenitor Cells by Trapping Unphosphorylated STAT3
1757 in the Nucleus. *J Virol* 92, e00340-18. <https://doi.org/10.1128/JVI.00340-18>.
- 1758 111. Yu, M., Zhang, X., Wang, Z., Wang, S., Li, J., Huang, H., Li, X., Wang, C., Shen, W., Sun,
1759 W., et al. (2025). Brain-specific expression of cytomegalovirus immediate early protein 1
1760 disrupts neurodevelopment in mice by inducing neuroinflammation and altering astrocytic
1761 metabolism. *Virol J* 22, 258. <https://doi.org/10.1186/s12985-025-02874-9>.
- 1762 112. Scheffner, M., Werness, B.A., Huibregtse, J.M., Levine, A.J., and Howley, P.M. (1990).
1763 The E6 oncoprotein encoded by human papillomavirus types 16 and 18 promotes the
1764 degradation of p53. *Cell* 63, 1129–1136. [https://doi.org/10.1016/0092-8674\(90\)90409-8](https://doi.org/10.1016/0092-8674(90)90409-8).

- 1765 113. Dyson, N., Howley, P.M., Münger, K., and Harlow, E. (1989). The human papilloma virus-
1766 16 E7 oncoprotein is able to bind to the retinoblastoma gene product. *Science* 243, 934–
1767 937. <https://doi.org/10.1126/science.2537532>.
- 1768 114. Alcami, A., and Koszinowski, U.H. (2000). Viral mechanisms of immune evasion. *Trends*
1769 *Microbiol* 8, 410–418. [https://doi.org/10.1016/s0966-842x\(00\)01830-8](https://doi.org/10.1016/s0966-842x(00)01830-8).
- 1770 115. You, H., Zheng, S., Huang, Z., Lin, Y., Shen, Q., and Zheng, C. (2019). Herpes Simplex
1771 Virus 1 Tegument Protein UL46 Inhibits TANK-Binding Kinase 1-Mediated Signaling. *mBio*
1772 10, e00919-19. <https://doi.org/10.1128/mBio.00919-19>.
- 1773 116. Boomker, J.M., van Luyn, M.J.A., The, T.H., de Leij, L.F.M.H., and Harmsen, M.C. (2005).
1774 US28 actions in HCMV infection: lessons from a versatile hijacker. *Rev Med Virol* 15, 269–
1775 282. <https://doi.org/10.1002/rmv.468>.
- 1776 117. Doorbar, J., Egawa, N., Griffin, H., Kranjec, C., and Murakami, I. (2015). Human
1777 papillomavirus molecular biology and disease association. *Rev Med Virol* 25 *Suppl* 1, 2–
1778 23. <https://doi.org/10.1002/rmv.1822>.
- 1779 118. Doorbar, J. (2006). Molecular biology of human papillomavirus infection and cervical
1780 cancer. *Clin Sci (Lond)* 110, 525–541. <https://doi.org/10.1042/CS20050369>.
- 1781 119. Shirinian, M., Kfoury, Y., Dassouki, Z., El-Hajj, H., and Bazarbachi, A. (2013). Tax-1 and
1782 Tax-2 similarities and differences: focus on post-translational modifications and NF-κB
1783 activation. *Front Microbiol* 4, 231. <https://doi.org/10.3389/fmicb.2013.00231>.
- 1784 120. Chevalier, S.A., Durand, S., Dasgupta, A., Radonovich, M., Cimarelli, A., Brady, J.N.,
1785 Mahieux, R., and Pise-Masison, C.A. (2012). The transcription profile of Tax-3 is more
1786 similar to Tax-1 than Tax-2: insights into HTLV-3 potential leukemogenic properties. *PLoS*
1787 *One* 7, e41003. <https://doi.org/10.1371/journal.pone.0041003>.
- 1788 121. Reece-Hoyes, J.S., Diallo, A., Lajoie, B., Kent, A., Shrestha, S., Kadreppa, S., Pesyna, C.,
1789 Dekker, J., Myers, C.L., and Walhout, A.J.M. (2011). Enhanced yeast one-hybrid assays
1790 for high-throughput gene-centered regulatory network mapping. *Nat Methods* 8, 1059–
1791 1064. <https://doi.org/10.1038/nmeth.1748>.
- 1792 122. Berenson, A., and Fuxman Bass, J.I. (2023). Enhanced Yeast One-Hybrid Assays to Study
1793 Protein-DNA Interactions. *Methods Mol Biol* 2599, 11–20. https://doi.org/10.1007/978-1-0716-2847-8_2.
- 1795 123. Shrestha, S., Liu, X., Santoso, C.S., and Fuxman Bass, J.I. (2019). Enhanced Yeast One-
1796 hybrid Screens To Identify Transcription Factor Binding To Human DNA Sequences. *J Vis*
1797 *Exp*. <https://doi.org/10.3791/59192>.
- 1798 124. Fuxman Bass, J.I., Reece-Hoyes, J.S., and Walhout, A.J.M. (2016). Performing Yeast
1799 One-Hybrid Library Screens. *Cold Spring Harb Protoc* 2016, pdb.prot088955.
1800 <https://doi.org/10.1101/pdb.prot088955>.
- 1801 125. Lu, Y., Berenson, A., Lane, R., Guelin, I., Li, Z., Chen, Y., Shah, S., Yin, M., Soto-Ugaldi,
1802 L.F., Fiszbein, A., et al. (2024). A large-scale cancer-specific protein-DNA interaction
1803 network. *Life Sci Alliance* 7, e202402641. <https://doi.org/10.26508/lsa.202402641>.

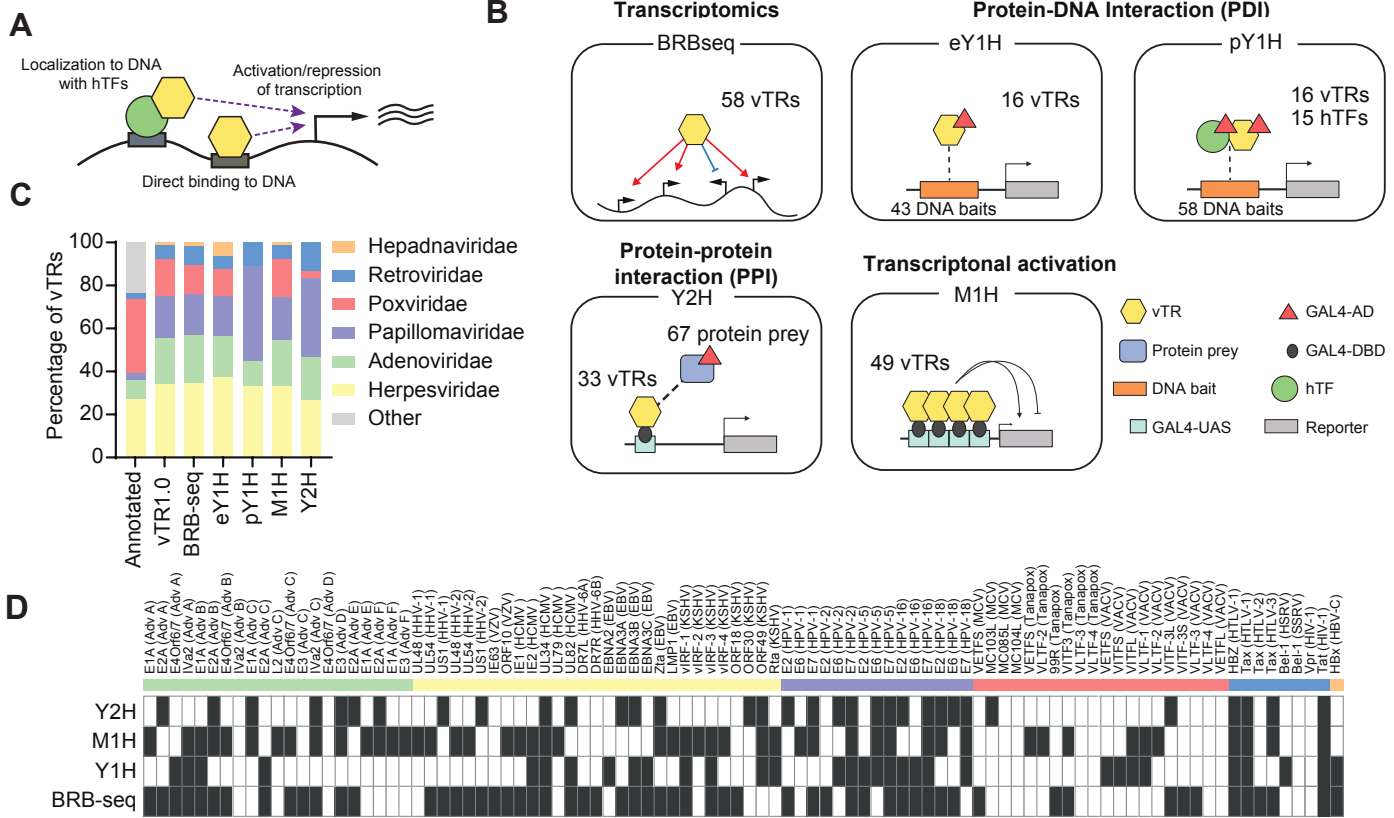
- 1804 126. Schlabach, M.R., Hu, J.K., Li, M., and Elledge, S.J. (2010). Synthetic design of strong
1805 promoters. *Proc Natl Acad Sci U S A* 107, 2538–2543.
1806 <https://doi.org/10.1073/pnas.0914803107>.
- 1807 127. Frenkel, M., Corban, J.E., Hujuel, M.L.A., Morris, Z., and Raman, S. (2025). Large-scale
1808 discovery of chromatin dysregulation induced by oncofusions and other protein-coding
1809 variants. *Nat Biotechnol* 43, 996–1010. <https://doi.org/10.1038/s41587-024-02347-4>.
- 1810 128. Luck, K., Kim, D.-K., Lambourne, L., Spirohn, K., Begg, B.E., Bian, W., Brignall, R.,
1811 Cafarelli, T., Campos-Laborie, F.J., Charlotteaux, B., et al. (2020). A reference map of the
1812 human binary protein interactome. *Nature* 580, 402–408. [https://doi.org/10.1038/s41586-](https://doi.org/10.1038/s41586-020-2188-x)
1813 [020-2188-x](https://doi.org/10.1038/s41586-020-2188-x).
- 1814 129. Mudge, J.M., Carbonell-Sala, S., Diekhans, M., Martinez, J.G., Hunt, T., Jungreis, I.,
1815 Loveland, J.E., Arnan, C., Barnes, I., Bennett, R., et al. (2025). GENCODE 2025:
1816 reference gene annotation for human and mouse. *Nucleic Acids Res* 53, D966–D975.
1817 <https://doi.org/10.1093/nar/gkae1078>.
- 1818 130. Dobin, A., Davis, C.A., Schlesinger, F., Drenkow, J., Zaleski, C., Jha, S., Batut, P.,
1819 Chaisson, M., and Gingeras, T.R. (2013). STAR: ultrafast universal RNA-seq aligner.
1820 *Bioinformatics* 29, 15–21. <https://doi.org/10.1093/bioinformatics/bts635>.
- 1821 131. Hao, Y., Stuart, T., Kowalski, M.H., Choudhary, S., Hoffman, P., Hartman, A., Srivastava,
1822 A., Molla, G., Madad, S., Fernandez-Granda, C., et al. (2024). Dictionary learning for
1823 integrative, multimodal and scalable single-cell analysis. *Nat Biotechnol* 42, 293–304.
1824 <https://doi.org/10.1038/s41587-023-01767-y>.
- 1825 132. Love, M.I., Huber, W., and Anders, S. (2014). Moderated estimation of fold change and
1826 dispersion for RNA-seq data with DESeq2. *Genome Biol* 15, 550.
1827 <https://doi.org/10.1186/s13059-014-0550-8>.
- 1828 133. Subramanian, A., Tamayo, P., Mootha, V.K., Mukherjee, S., Ebert, B.L., Gillette, M.A.,
1829 Paulovich, A., Pomeroy, S.L., Golub, T.R., Lander, E.S., et al. (2005). Gene set enrichment
1830 analysis: a knowledge-based approach for interpreting genome-wide expression profiles.
1831 *Proc Natl Acad Sci U S A* 102, 15545–15550. <https://doi.org/10.1073/pnas.0506580102>.
- 1832 134. Liberzon, A., Birger, C., Thorvaldsdóttir, H., Ghandi, M., Mesirov, J.P., and Tamayo, P.
1833 (2015). The Molecular Signatures Database (MSigDB) hallmark gene set collection. *Cell*
1834 *Syst* 1, 417–425. <https://doi.org/10.1016/j.cels.2015.12.004>.
- 1835 135. Abramson, J., Adler, J., Dunger, J., Evans, R., Green, T., Pritzel, A., Ronneberger, O.,
1836 Willmore, L., Ballard, A.J., Bambrick, J., et al. (2024). Accurate structure prediction of
1837 biomolecular interactions with AlphaFold 3. *Nature* 630, 493–500.
1838 <https://doi.org/10.1038/s41586-024-07487-w>.
- 1839 136. Pettersen, E.F., Goddard, T.D., Huang, C.C., Meng, E.C., Couch, G.S., Croll, T.I., Morris,
1840 J.H., and Ferrin, T.E. (2021). UCSF ChimeraX: Structure visualization for researchers,
1841 educators, and developers. *Protein Sci* 30, 70–82. <https://doi.org/10.1002/pro.3943>.
- 1842 137. Shen, W.-K., Chen, S.-Y., Gan, Z.-Q., Zhang, Y.-Z., Yue, T., Chen, M.-M., Xue, Y., Hu, H.,
1843 and Guo, A.-Y. (2023). AnimalTFDB 4.0: a comprehensive animal transcription factor

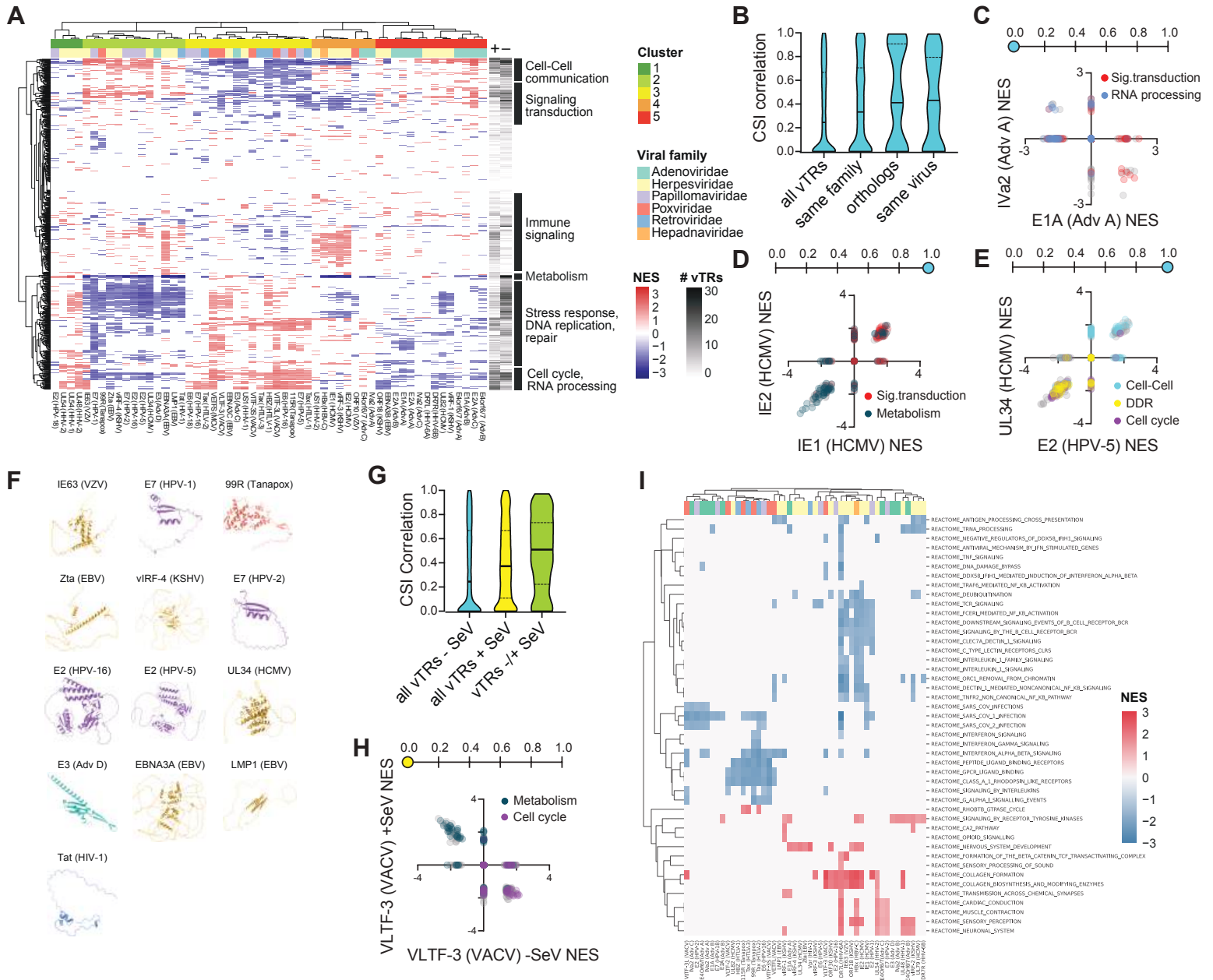
1844 database updated with variation and expression annotations. *Nucleic Acids Res* 51, D39–
1845 D45. <https://doi.org/10.1093/nar/gkac907>.

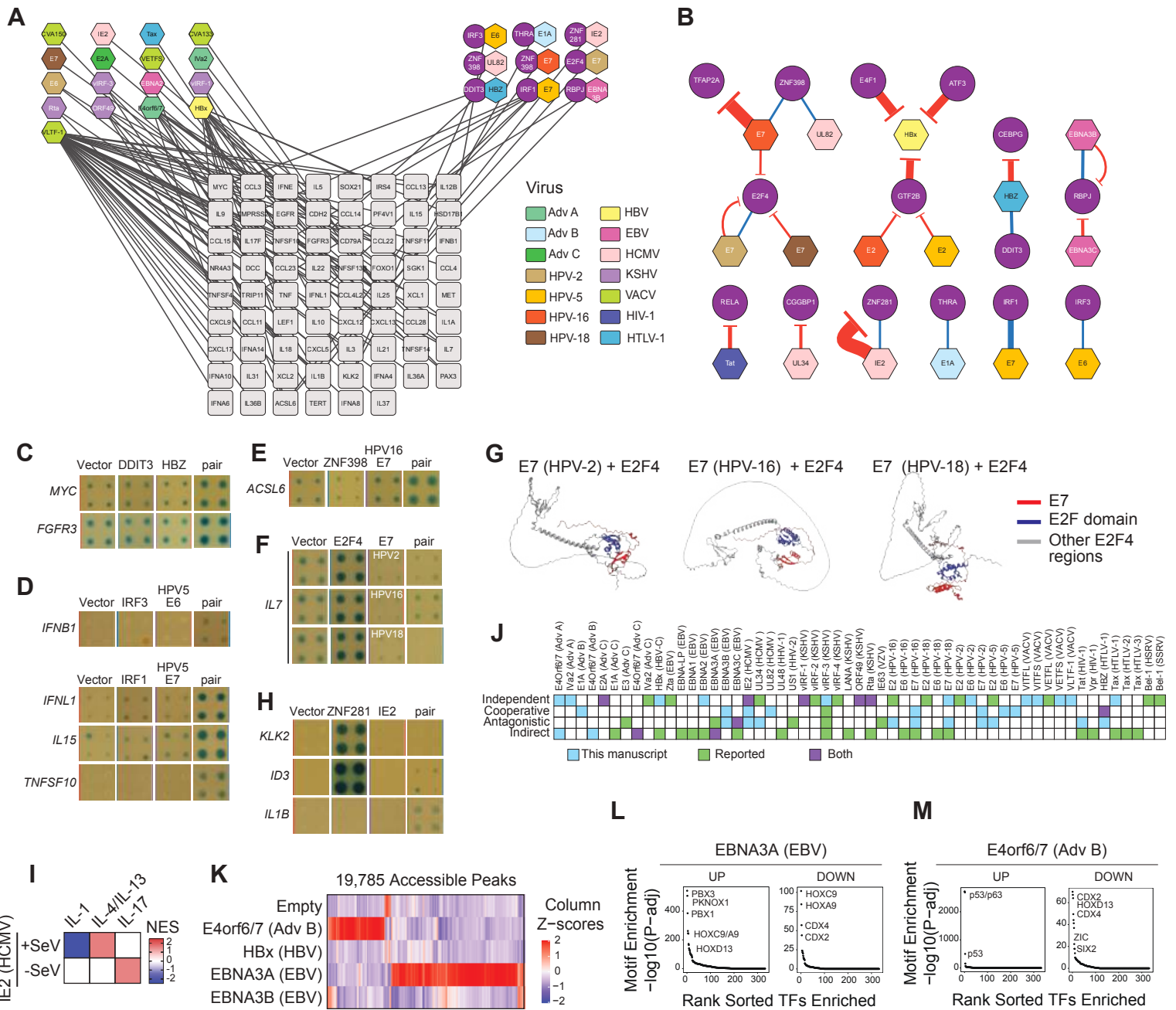
1846 138. Oughtred, R., Rust, J., Chang, C., Breitkreutz, B.-J., Stark, C., Willems, A., Boucher, L.,
1847 Leung, G., Kolas, N., Zhang, F., et al. (2021). The BioGRID database: A comprehensive
1848 biomedical resource of curated protein, genetic, and chemical interactions. *Protein Sci* 30,
1849 187–200. <https://doi.org/10.1002/pro.3978>.

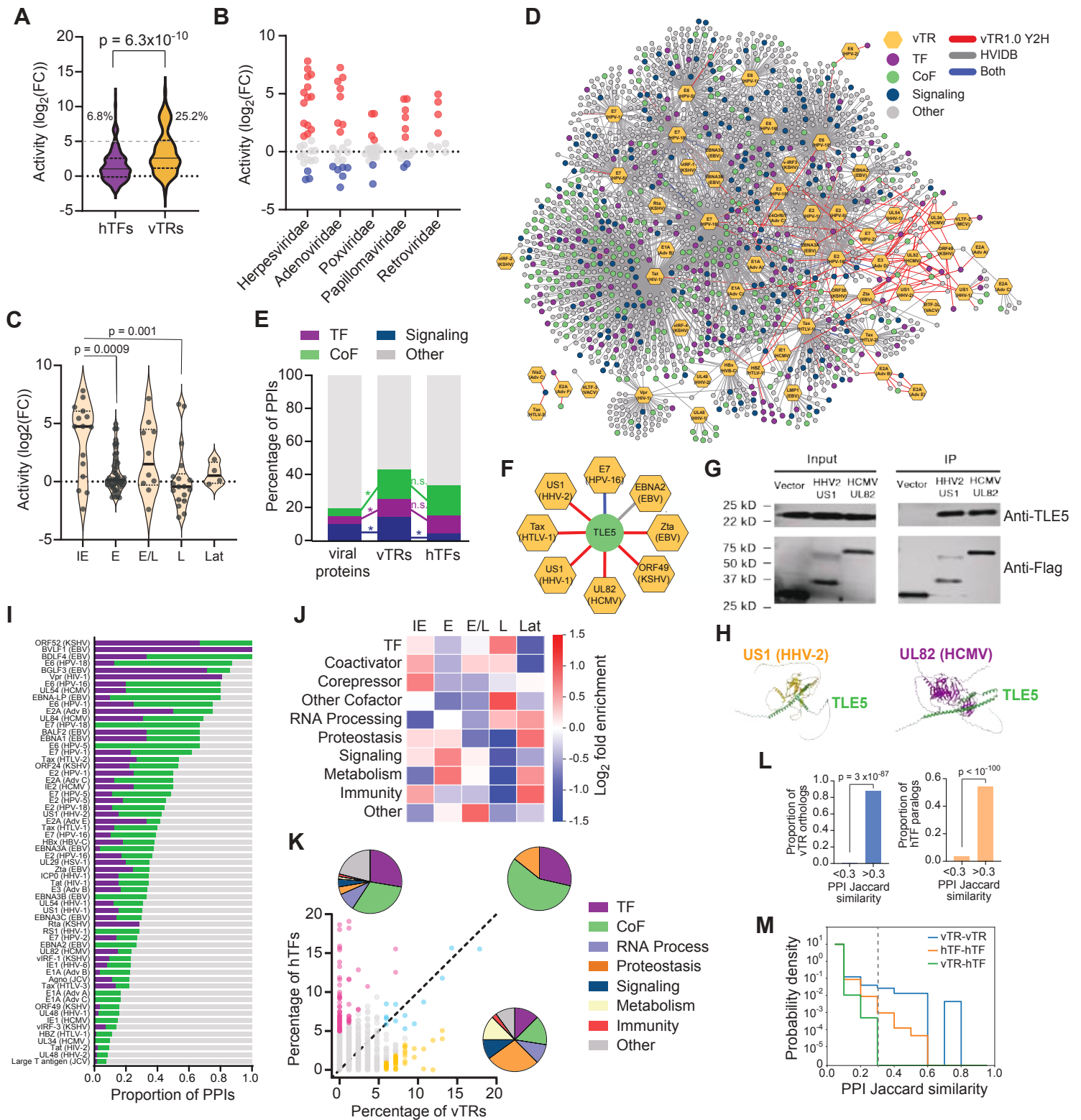
1850

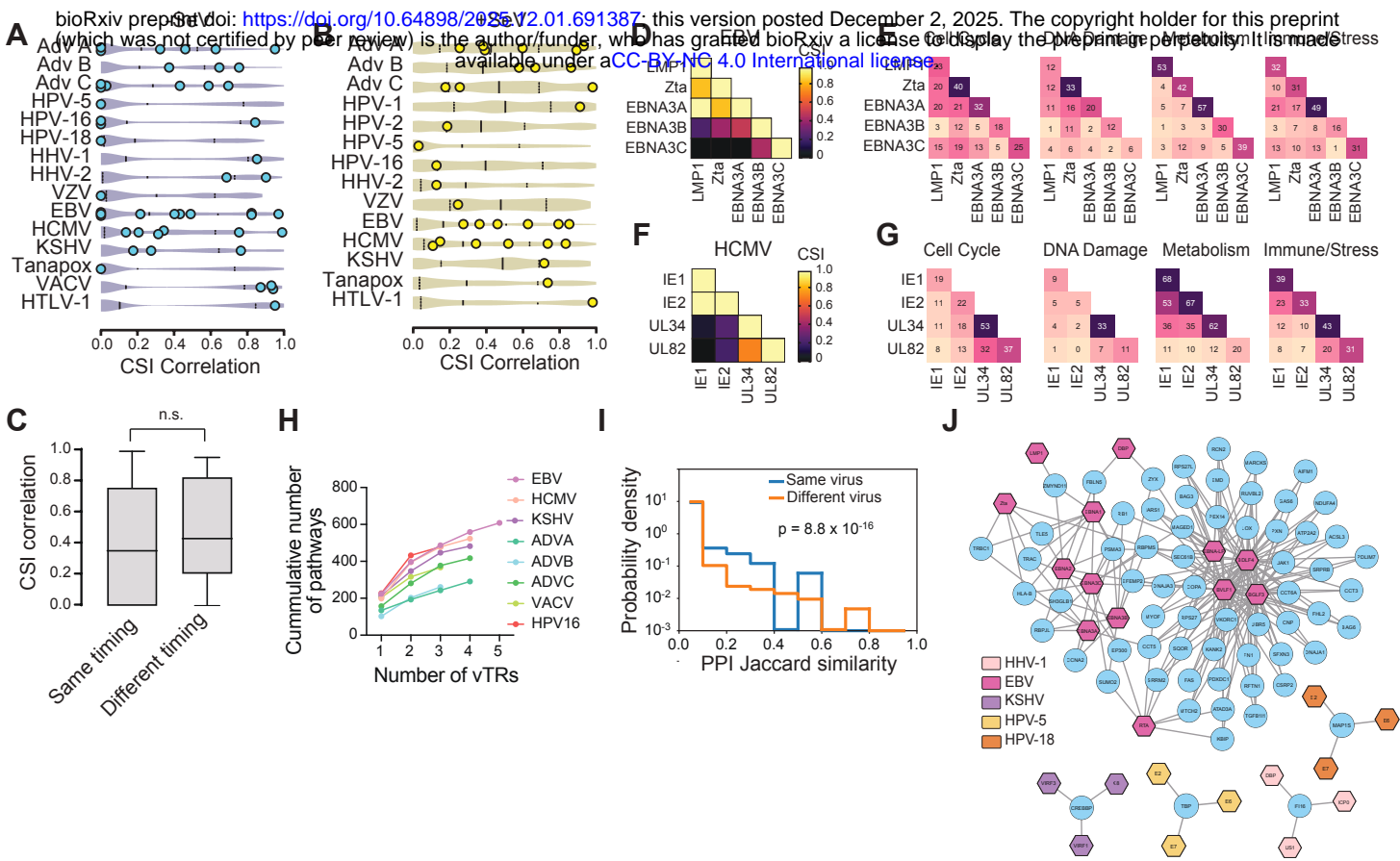
1851

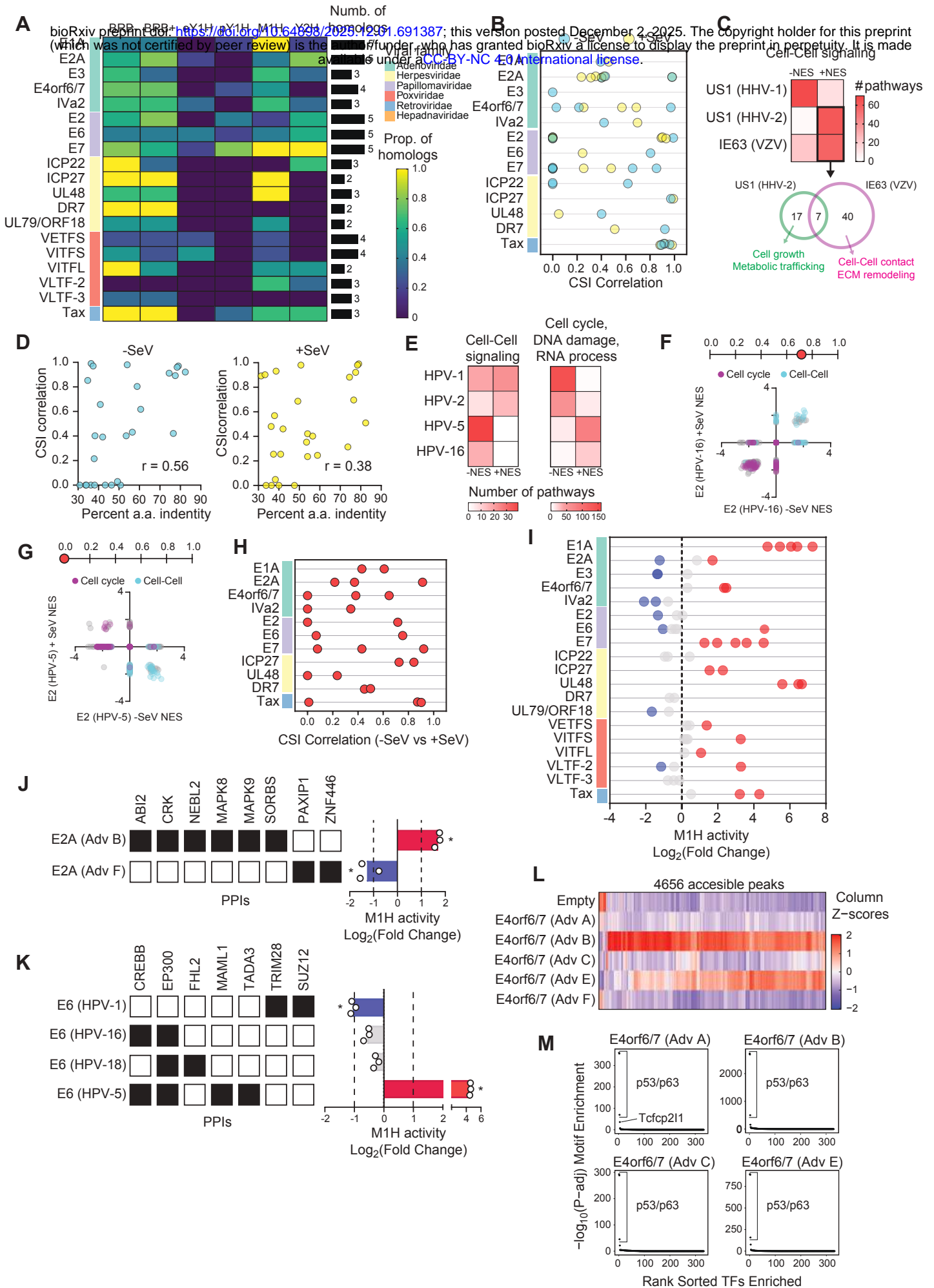


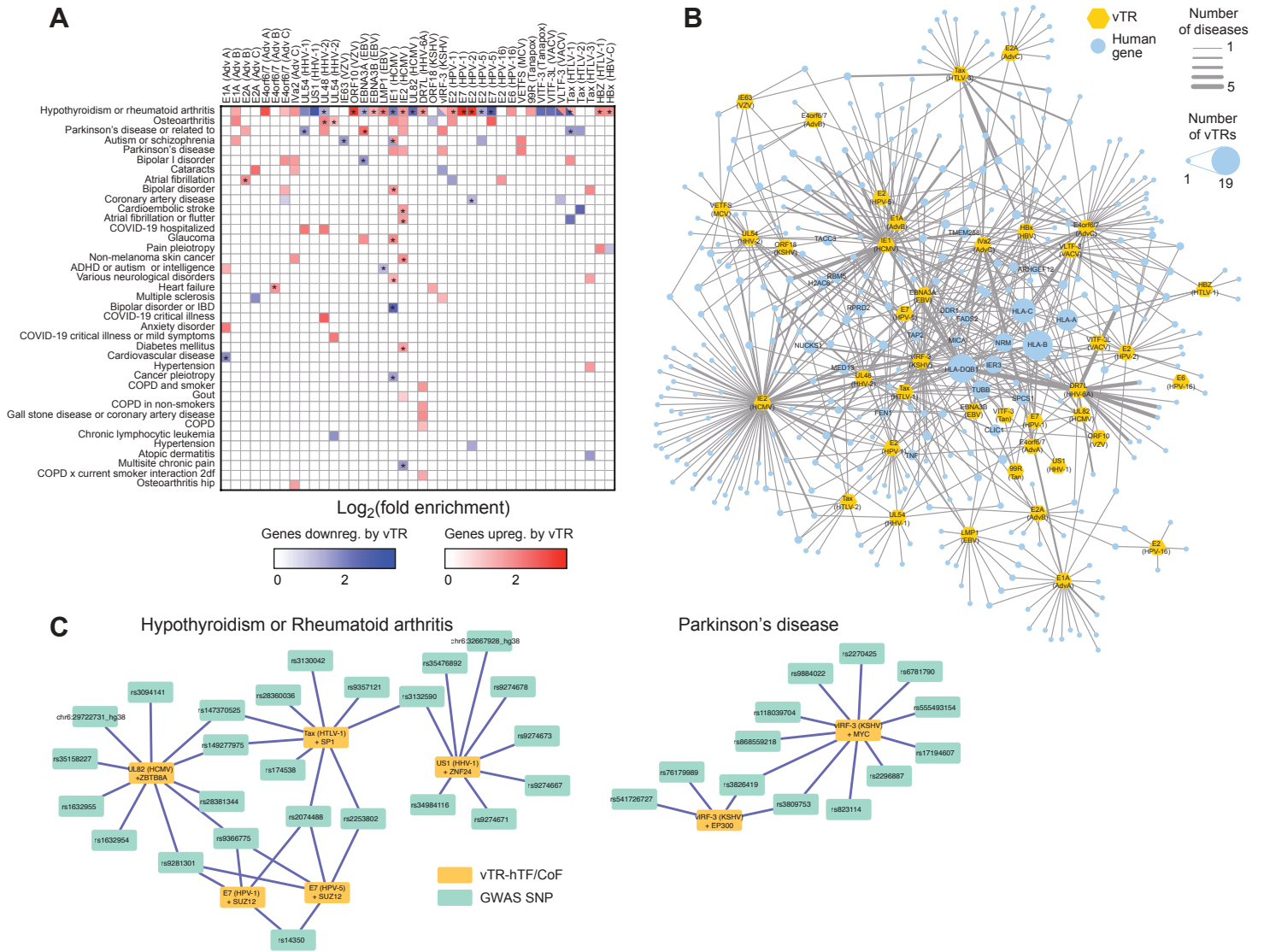


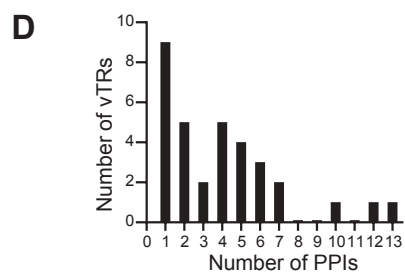
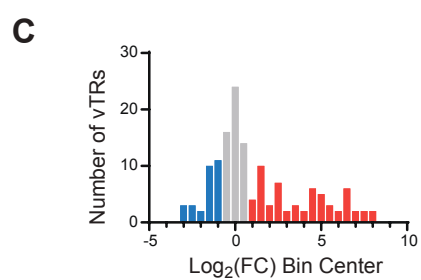
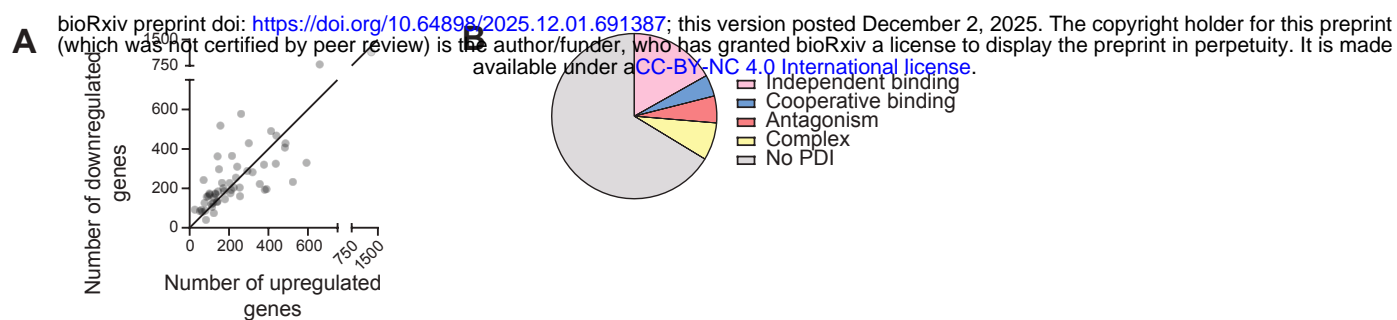


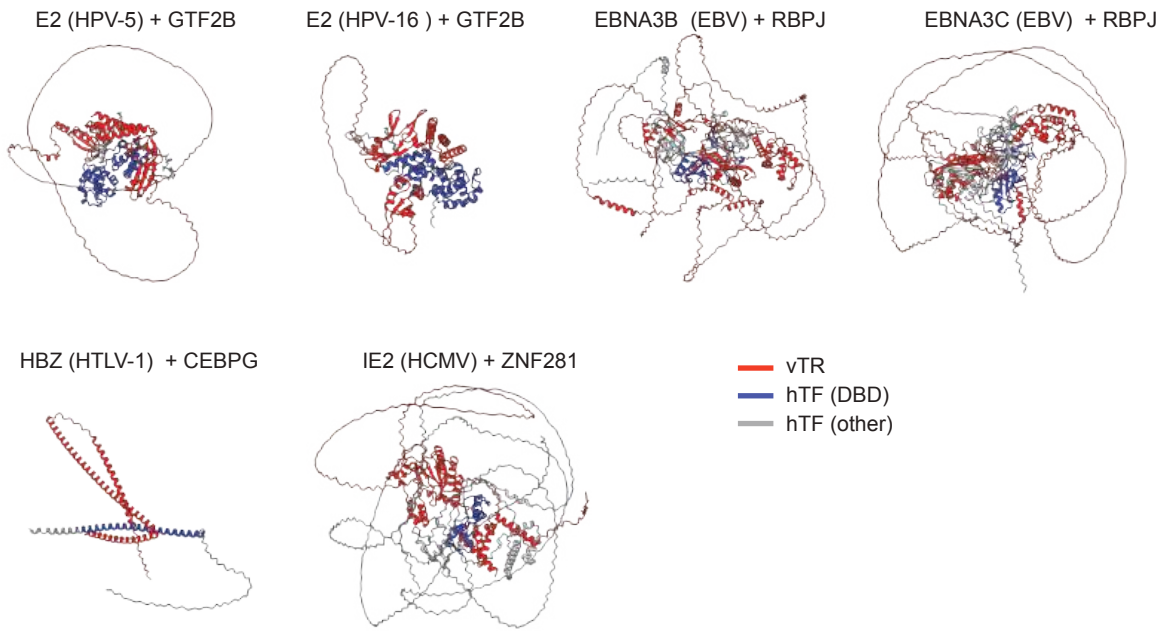












bioRxiv preprint doi: <https://doi.org/10.64898/2025.12.01.691387>; this version posted December 2, 2025. The copyright holder for this preprint (which was not certified by peer review) is the author/funder, who has granted bioRxiv a license to display the preprint in perpetuity. It is made available under a [CC-BY-NC 4.0 International license](#).

